SECURITY INFORMATION

CONFIDENTIAL

Copy 284
RM L52I23

NACA RM L52I23

NACA

RESEARCH MEMORANDUM

THE EFFECTS OF SWEEPBACK ON LONGITUDINAL CHARACTERISTICS OF A $\frac{1}{30}$-SCALE SEMISPAN MODEL OF THE BELL X-5 AIRPLANE AS DETERMINED FROM NACA WING-FLOW TESTS AT TRANSONIC SPEEDS

By Joseph J. Kolnick and Robert M. Kennedy

Langley Aeronautical Laboratory
Langley Field, Va.

CLASSIFICATION CHANGED TO UNCLASSIFIED

AUTHORITY NACA RESEARCH ABSTRACT NO. 94

CLASSIFIED DOCUMENT

DATE Jan 17, 1956 WHL

This material contains information affecting the National Defense of the United States within the meaning of the espionage laws, Title 18, U.S.C., Secs. 793 and 794, the transmission or revelation of which in any manner to unauthorized person is prohibited by law.

NATIONAL ADVISORY COMMITTEE FOR AERONAUTICS

WASHINGTON

November 14, 1952

CONFIDENTIAL

NATIONAL ADVISORY COMMITTEE FOR AERONAUTICS

RESEARCH MEMORANDUM

THE EFFECTS OF SWEEPBACK ON LONGITUDINAL CHARACTERISTICS OF A $\frac{1}{30}$-SCALE SEMISPAN MODEL OF THE BELL X-5 AIRPLANE AS DETERMINED FROM NACA WING-FLOW TESTS AT TRANSONIC SPEEDS

By Joseph J. Kolnick and Robert M. Kennedy

SUMMARY

Tests were made by the NACA wing-flow method to determine the effect of sweepback angle on the longitudinal characteristics of a $\frac{1}{30}$-scale semispan model of the Bell X-5 variable-sweep airplane at Mach numbers from 0.70 to 1.05. Lift, drag, and pitching moments were obtained through an angle-of-attack range of -4° to 12°. The Reynolds number of the tests was 1.3×10^6 ±8 percent based on the mean aerodynamic chord of the 60° swept wing. Tests were made with the wings of the model in the 20°, 30°, 40°, 50°, and 60° sweptback positions and with a tail incidence of -2°. The characteristics of the fuselage alone were also determined.

The results of the tests indicated that the lift coefficient at which stall occurred increased with an increase in sweep at least for Mach numbers from 0.75 to 0.90. The lift-curve slope decreased with an increase in sweep angle for all test Mach numbers except for the range between 0.80 and 0.90.

By assuming level flight at 40,000 feet and a wing loading of 50, it appears that the sweep angle for least drag would increase from 30° to 40° as the Mach number was increased from 0.75 to 0.83, from 40° to 50° for Mach numbers from 0.83 to 0.92, and from 50° to 60° as the Mach number was increased to about 1.00.

The 20°, 30°, 40°, and 50° sweep settings showed a longitudinal instability occurring at lift coefficients above 0.5 for Mach numbers below 0.90 and 0.95. For the 60° sweep setting, moment data were not

obtained at sufficiently high lift coefficients to indicate whether instability would be encountered.

In general, even with forward translation of the wing accompanying the increase from 20° to 60° sweep angle, the stability of the model increased with increasing sweep at all Mach numbers.

INTRODUCTION

As part of a program to determine the aerodynamic characteristics of the Bell X-5 research airplane incorporating a wing for which the angle of sweep can be varied in flight, an investigation was made at transonic speeds by the NACA wing-flow method on a $\frac{1}{30}$-scale semispan model of a preliminary configuration.

Results of tests covering several phases of investigations at low supersonic Mach numbers have been reported in references 1 to 4. The present paper is the first of a series reporting aerodynamic characteristics within the transonic speed range (Mach numbers from 0.70 to 1.05). Results of measurements of normal force, chord force, and pitching moment are presented for a semispan model with the wing sweptback 20°, 30°, 40°, 50°, and 60°, and a tail incidence of -2°. Similar measurements were also made of the fuselage alone.

SYMBOLS

V	velocity, ft/sec
S	model wing area, semispan (includes area in fuselage between perpendiculars from wing-fuselage intersection to plane of symmetry), sq ft
L	lift force, lb
D	drag force, lb
M	pitching moment, in.-lb
R_w	Reynolds number based on mean aerodynamic chord of 60° swept wing
R_t	Reynolds number based on $\bar{c}_t$

C_L lift coefficient, L/qS

C_D drag coefficient, D/qS

C_{D_o} drag coefficient at zero lift

C_m pitching-moment coefficient, $M/qS\bar{c}$

M_L local Mach number at wing surface of North American F-51D airplane

M_W effective Mach number for wing of model

M_t effective Mach number for tail of model

$\bar{c}$ mean aerodynamic chord of wing; based on relationship $\dfrac{\int_o^{b/2} c^2\,dy}{\int_o^{b/2} c\,dy}$ where b is wing span, c is chord, and y is spanwise coordinate, in.

q effective dynamic pressure for wing of model, $\frac{1}{2}\rho V^2$, lb/sq ft

$\bar{c}_t$ mean aerodynamic chord of tail, in.

i_t incidence of horizontal tail (referred to wing-chord plane)

α angle of attack of fuselage, deg

ρ mass density, slugs/cu ft

Λ sweepback angle referred to 25-percent-chord line, deg

$dC_L/d\alpha$ variation of lift coefficient with angle of attack, per deg

dC_M/dC_L variation of pitching-moment coefficient with lift coefficient

Prime indicates coefficients based on dimensions of configuration with 60° sweptback wing.

MODEL AND TESTS

Model.- The configurations tested and reported consisted of a preliminary $\frac{1}{30}$-scale semispan model of the X-5 airplane equipped successively with wings of 20°, 30°, 40°, 50°, and 60° sweepback angles referred to the 25-percent-chord line. For the present investigation the horizontal tail incidence was -2°. A test was also made for the fuselage alone.

A photograph of the semispan model equipped with end plate is shown in figure 1; photograph of the model with the wing swept back 20° is shown in figure 2. The geometric characteristics of the model are given in table I; other details of the model are shown in figure 3. The geometry and dimensions of the wing with different sweepback angles are shown in figure 4. The airfoil section perpendicular to the unswept 39-percent-chord line (wing pivot point of the full-scale airplane) was an NACA $64_{(10)}$A011 at the root (through the pivot point) and tapered to NACA $64_{(08)}$A008.6 at the tip. The horizontal tail had an NACA 64A006 airfoil section parallel to the free stream and was sweptback 45° along the 25-percent-chord line. The aspect ratios of the 20°, 30°, 40°, 50°, and 60° swept wings are, respectively, 4.82, 4.44, 3.77, 2.98, and 2.18 when the end plate is considered as a reflection plane. The wing and tail surfaces of the model were fabricated from solid duralumin, whereas the fuselage was of mahogany reinforced with duralumin. A duct was included in the fuselage of the model to simulate to some extent the air intake and flow through the jet engine of the full-scale airplane.

The model was originally designed and constructed so that the pitching moment would be measured about the 25-percent mean-aerodynamic-chord location (gross-weight center-of-gravity location of the full-scale airplane) of the wing in each sweep position. To keep the pitching moment about the 25-percent mean aerodynamic chord on the original model, the wing was translated forward as the sweep increased from 20° to 50° and was translated backwards somewhat as the sweep increased from 50° to 60°. However, with subsequent changes in wing span and fillets on the model, the positions about which the pitching moments were measured actually correspond to the 35-, 36-, 35, 29-, and 26-percent mean aerodynamic chords of the 20°, 30°, 40°, 50°, and 60° swept wings, respectively. The model tested differs from the full-scale configuration only in having different wing fillets and in the longitudinal location of the wing for the various sweep angles. The semispan model, which was shaped along the fuselage center line to conform to the curvature of the airplane wing in the test region, was mounted close to the North American F-51D modified wing surface and was connected to a balance enclosed within the wing.

Tests.- The investigation was made by the NACA wing-flow method in which the model is mounted in the region of high-speed flow over the wing of an F-51D airplane.

The model and balance were arranged to oscillate as a unit so that the forces were measured normal and parallel to the fuselage reference line of the model at all angles of attack. Continuous measurements were made of angle of attack, normal force, chord force, and pitching moment as the model oscillated 3/4 cycle per second through an angle-of-attack range of -4° to 12°. The angle of attack was determined from measurements of model angle and local flow angle. The local flow angle was determined from a free-floating vane mounted outboard of the model station as described in reference 5.

The chordwise velocity gradients in the test region on the airplane wing determined from static-pressure measurements at the wing surface with the model removed are indicated in figure 5. The vertical gradient over the entire test section was -0.004 Mach number per inch. The effective dynamic pressure q, the effective Mach number for the various model wings M_W, and the effective Mach number at the model tail M_t were determined from an integration of the velocity distribution over the area covered by the wing and the tail of the model, respectively. The variation of Mach number for the tail M_t with Mach number for the wings M_W, due to the chordwise velocity gradient, is shown in figure 6. A more complete discussion of the method for determining the Mach number and dynamic pressure at the model can be found in reference 5.

The tests were made by diving the F-51D airplane from an altitude of about 24,000 feet to approximately 14,000 feet, at which altitude an airplane Mach number of 0.75 was obtained and the recording instruments started. The dive was then continued at an indicated speed of 450 miles per hour and a pullout to level flight effected at an altitude of 5000 feet. In the level-flight portion of the test the airplane was allowed to decelerate to an airplane Mach number of 0.5, at which time the recording instruments were discontinued. This test procedure permits the maximum Reynolds number to be obtained at a given Mach number within the placard limits of the airplane.

The average relation between Reynolds number of the 60° wing R_W and the Reynolds number of the tail R_T with Mach number at the wing M_W is shown in figure 7. The Reynolds number for wings other than the 60° wing can be found by multiplying the values of R_W in figure 7 by the ratio of the $\bar{c}$ of the wing desired to the $\bar{c}$ of the 60° wing.

PRESENTATION OF RESULTS

For figures 8 to 12, the lift, drag, and pitching-moment characteristics are based on the area of the wing extending to the plane of symmetry as shown in figure 4. All pitching moments are referred to the common fuselage station about which the measurements were taken. This station corresponded to the 35-, 36-, 35-, 29-, and 26-percent mean-aerodynamic-chord points of the 20°, 30°, 40°, 50°, and 60° swept wings, respectively.

Figure 8 shows sample data for one complete oscillation of the model through the angle-of-attack range. Pitching-moment data were obtained over part of the angle-of-attack range investigated because of limitations in the capacity of the pitching-moment element of the balance. Data are shown for both increasing and decreasing angles of attack for the cycle. During this particular cycle, the Mach number varied 0.002. The faired curves are used to give results for a Mach number of 0.90. Similarly, several cycles were worked up for each configuration through the Mach number range and cross-plotted to show variations of the characteristics with Mach number at constant lift coefficients as given in figure 9. Results from reference 3 at a Mach number of 1.24 are also shown in figure 9 and in figure 13(g) for the lift-curve slope for the 40°, 50°, and 60° wings. The dashed lines are used merely to connect proper data points at $M_W = 1.24$ from reference 3 and curves of the present tests.

Plots of C_L against α, C_L against C_D, and C_m against α, obtained from cross-plots of figure 9, are presented in figures 10, 11, and 12, respectively, for several Mach numbers.

The effects of a variable-sweep configuration on the drag coefficient at various lift coefficients, on the rate of change of pitching-moment coefficients with lift coefficient $dC_{m_{0.26\bar{c}'}}/dC_L'$, and on the rate of change of lift coefficient with angle of attack $dC_L'/d\alpha$ are shown in figure 13. All coefficients in this figure are based on the dimensions of the 60° wing in order to indicate the characteristics of the model as a variable-sweep configuration.

The characteristics of the model fuselage alone at constant angles of attack through the Mach number range are presented in figure 14, All coefficients in this figure are based on the dimensions of the 60° wing. Also shown are the data for the fuselage alone at a Mach number of 1.24 (ref. 2).

DISCUSSION

Lift.- The results in figure 9 indicate considerable variation, especially at the higher lift coefficient, in angle of attack at

constant lift coefficient or correspondingly in the lift-curve slope with Mach number for the 20° sweep angle. This variation became progressively less as the sweep was increased until at 60° sweep the lift-curve slope was practically independent of Mach number.

In figure 10, the results indicate a practically linear variation of lift coefficient with angle of attack in the unstalled range for the 20° and 30° sweep angles. At the higher sweep angles the slopes increase with an increase in lift coefficient. With the 20° and 30° sweep angles, stall begins at a lift coefficient of about 0.5 for Mach numbers from 0.75 to 0.90. For Mach numbers above 0.90 the stall did not occur up to a lift coefficient of 0.6 which was the limit of the tests. At the higher sweep angles there was no marked indication of stalling within the lift-coefficient range of the tests at any Mach number.

The variation of lift-curve slope with sweep given in figure 13 shows for zero-lift coefficient a progressive decrease with increasing sweep angle for test Mach numbers below 0.80 and above 0.95. For zero-lift coefficient there is a deterioration in the lift-curve slope between Mach numbers of 0.80 and 0.95 for the 20° sweep and between Mach numbers of 0.85 and 0.95 for the 30° sweep so that at a Mach number of 0.90 the 40° sweep angle gives the highest lift-curve slope. For 0.4 lift coefficient the same conditions exist as for zero-lift coefficient except the lift-curve deterioration occurs only for the 20° sweep angle and begins at an earlier Mach number of 0.80. The results reproduced in figure 13(g) from reference 3 indicate little variation in lift-curve slope between Mach numbers of 1.03 and 1.24 for the 40° to 60° sweep angles.

As shown in figure 14, the variation of lift coefficient with angle of attack for the fuselage alone has a small approximately constant value throughout the Mach number range tested and amounts to about 5 percent of the lift-curve slope of the complete model with 60° sweep and zero-lift coefficient.

Drag.- The absolute values of drag coefficients presented are considered qualitative because they are subject to unknown effects of the reflection-plane method of testing on the drag of the model fuselage and include the drag of the end plate. However, the variation of drag coefficient with lift coefficient and Mach number, and the differences between the drag coefficients for the various configurations are believed to be unaffected by these factors.

The drag-rise Mach number of the model indicated in figure 9 is not too well-defined, but it appears to increase from about 0.80 with 20° sweep to about 0.90 with 50° sweep for zero-lift coefficient. Above 50° sweep there is little change in the drag rise Mach number apparently because the drag rise is associated primarily with the fuselage rather than the wing. The results given in figure 14 indicate that the drag rise for the fuselage alone occurs at about a Mach number of 0.90. The

rise in drag coefficient from a Mach number of 0.80 to 1.02 at zero-lift coefficient decreased from a value of 0.073 for 20° sweep to 0.041 for the 60° sweep. The fuselage alone contributed a rise of 0.024 included in these amounts.

The drag due to lift indicated in figures 9 and 11 for any one Mach number and up to a lift coefficient of 0.4 is about the same for the 20° and 30° sweep angles and increases as the sweep angle is increased to 60°. When the Mach number is varied from 0.75 to 0.90 the drag due to lift for the 20° and 30° sweep settings approximately doubles and then decreases somewhat with further increase in Mach number. However, Mach number appears to have no marked effect on the drag due to lift of the 50° and 60° sweep settings.

The results in figure 13 indicate the sweep angles that should give the least drag for the various conditions of Mach number and lift coefficient covered by the tests. For conditions of level flight at 40,000 feet with a wing loading of 50 pounds per square foot the sweep angle for least drag would increase from 30° to 40° as the Mach number is increased from 0.75 to 0.83, from 40° to 50° for Mach numbers from 0.83 to 0.92, and from 50° to 60° as the Mach number is increased further to about 1.00. The reduction in drag from 50° to 60° sweep angle was relatively small in comparison to that from 40° to 50° sweep angle.

The rather large differences in drag between the 20° and 30° sweep angles which appear in figure 13 for even the lowest Mach number of 0.75 is only partly accounted for by the greater exposed area of the 20° configuration. The drag results of the 20° sweep settings are considered questionable because incomplete results of several other tests of the model differing only in tail setting indicated considerably less drag.

Pitching moment.- From the results in figure 9, it appears that at any one Mach number for the 20° sweep there was little variation in stability dC_M/dC_L with lift coefficient, as indicated by the even spacing of the curves up to a lift coefficient of 0.6, even though at the lower Mach numbers stall began at a lift coefficient around 0.5, as shown in figure 10. However, a considerable increase in stability with increasing Mach number is indicated for the 20° and 30° sweep angles by the increased spacing of the curves. At lift coefficients above 0.5, instability dC_M/dC_L due to the falling off of the lift-curve slope occurred around 0.80 Mach number for the 30° sweep and around 0.90 Mach number for the 40° sweep.

At angles of attack corresponding to lift coefficients above 0.5 and Mach numbers below 0.90, the results in figure 12 indicate for the 20° sweep angle an instability from the value of $dC_M/d\alpha$ which corresponds to the decrease in the lift-curve slope shown in figure 10 even

though the value of dC_M/dC_L showed no instability. The 30° and 40° sweep angles showed instability, whereas the 50° sweep angle showed a tendency to instability in the lower Mach number range and lift coefficients above 0.5. In all cases at Mach numbers above 0.90 to 0.95, the unstable tendencies disappeared or perhaps were delayed to higher lift coefficients beyond the range of the tests. For the 60° sweep setting moment data were obtained only for lift coefficients up to 0.4 and any unstable condition that may exist was not reached. Up to this lift coefficient there was a marked increase in stability $dC_M/d\alpha$ with increasing lift coefficient throughout the Mach number range which was partly due to the increasing lift-curve slope (fig. 10).

The variation of pitching-moment slope with sweep in figure 13 indicates a general rearward movement of the aerodynamic center as the sweep angle was increased for the greater part of the Mach number range. These results indicate that the forward translational movement of the pivot of the wing as it is swept back should be somewhat greater than that used for the present model in order to obtain less variation in stability as the wing sweep is increased.

In figure 14, the variation of pitching-moment coefficient at constant angles of attack for the fuselage alone indicated relatively little Mach number effect and amounts to about 0.004 in terms of $dC_m'/d\alpha$.

CONCLUSIONS

Tests made by the NACA wing-flow method to determine the effect of sweepback angle on the longitudinal characteristics of a $\frac{1}{30}$-scale model of the Bell X-5 variable-sweep airplane at Mach numbers from 0.70 to 1.05 indicated the following results:

1. The lift coefficient at which stalling began increased with increasing sweep at least for Mach numbers from 0.75 to 0.90.

2. In general, the lift-curve slope decreased with an increasing sweep angle for all test Mach numbers except for the range between 0.80 and 0.90.

3. For the case of level flight at 40,000 feet with a wing loading of 50, it appeared that the sweep angle for least drag would increase from 30° to 40° as the Mach number was increased from 0.75 to 0.83, from 40° to 50° for Mach numbers from 0.83 to 0.92, and from 50° to 60° as the Mach number was increased to about 1.00.

4. The 20°, 30°, 40°, and 50° sweep settings showed longitudinal instability occurring at lift coefficients above 0.5 for Mach numbers below 0.90 to 0.95. For the 60° sweep setting, moment data were not obtained at sufficiently high lift coefficients to indicate whether instability would be encountered.

5. In general, even with forward translation of the wing accompanying the increase from 20° to 60° sweep angle, the stability of the model increased with increasing sweep at all Mach numbers.

Langley Aeronautical Laboratory,
National Advisory Committee for Aeronautics,
Langley Field, Va.

REFERENCES

1. Silsby, Norman S., Morris, Garland J., and Kennedy, Robert M.: Longitudinal Characteristics at Mach Number of 1.24 of a $\frac{1}{30}$-Scale Semispan Model of Bell X-5 Variable-Sweep Airplane with Wing Swept Back 60° From Tests by NACA Wing-Flow Method. NACA RM L50E02a, 1950.

2. Morris, Garland J., Kennedy, Robert M., and Silsby, Norman S.: The Effect of Sweepback on the Longitudinal Characteristics at a Mach Number of 1.24 of a $\frac{1}{30}$-Scale Semispan Model of the Bell X-5 Airplane From Tests by the NACA Wing-Flow Method. NACA RM L50I28, 1950.

3. Sawyer, Richard H., Kennedy, Robert M., and Morris, Garland J.: Longitudinal-Control Effectiveness and Downwash Characteristics at a Mach Number of 1.24 of a $\frac{1}{30}$-Scale Semispan Model of the Bell X-5 Airplane As Determined by the NACA Wing-Flow Method. NACA RM L50K15, 1951.

4. Kennedy, Robert M.: Effects of a Fuselage Flap Dive Brake on the Aerodynamic Characteristics of $\frac{1}{30}$-Scale Semispan Model of the Bell X-5 Variable-Sweep Airplane at a Mach Number 1.24 As Determined by the NACA Wing-Flow Method. NACA RM L50L11a, 1951.

5. Johnson, Harold I.: Measurements of Aerodynamic Characteristics of a 35° Sweptback NACA 65-009 Airfoil Model with a $\frac{1}{4}$-Chord Plain Flap by the NACA Wing-Flow Method. NACA RM L7F13, 1947.

TABLE I.- GEOMETRIC CHARACTERISTICS OF $\frac{1}{30}$-SCALE SEMISPAN

MODEL OF BELL X-5 VARIABLE-SWEEP AIRPLANE

Wing dimensions:					
Airfoil section (perpendicular to 38.58-percent-chord line)					
Root	NACA $64_{(10)}$A011				
Tip	NACA $64_{(08)}$008.6				
Sweepback angle, deg	20	30	40	50	60
Semispan, in.	6.18	5.82	5.31	4.60	3.88
Mean aerodynamic chord, in.	2.96	2.94	3.10	3.20	3.64
Chord at tip, in.	1.84	1.84	1.84	1.84	1.84
Chord at plane of symmetry, in.	4.50	4.40	4.40	4.50	4.25
Area (semispan), sq in.	15.84	15.30	14.97	14.20	13.79
Aspect ratio	4.82	4.44	3.77	3.98	2.18
Dihedral, deg	0	0	0	0	0
Incidence, deg	0	0	0	0	0

Horizontal tail:	
Section	NACA 64A006
Sweepback angle, deg	45
Semispan, in.	1.91
Mean aerodynamic chord, in.	1.43
Chord at tip, in.	0.72
Chord at plane of symmetry, in.	1.95
Area (semispan) sq in.	2.55
Aspect ratio	2.86
Height (above wing chord), in.	0.56
Length:	
From $0.26\bar{c}$ of 60° swept wing to $0.25\bar{c}_t$, in.	6.83
From $0.29\bar{c}$ of 50° swept wing to $0.25\bar{c}_t$, in.	6.83
From $0.35\bar{c}$ of 40° swept wing to $0.25\bar{c}_t$, in.	6.83
From $0.36\bar{c}$ of 30° swept wing to $0.25\bar{c}_t$, in.	6.83
From $0.35\bar{c}$ of 20° swept wing to $0.25\bar{c}_t$, in.	6.83

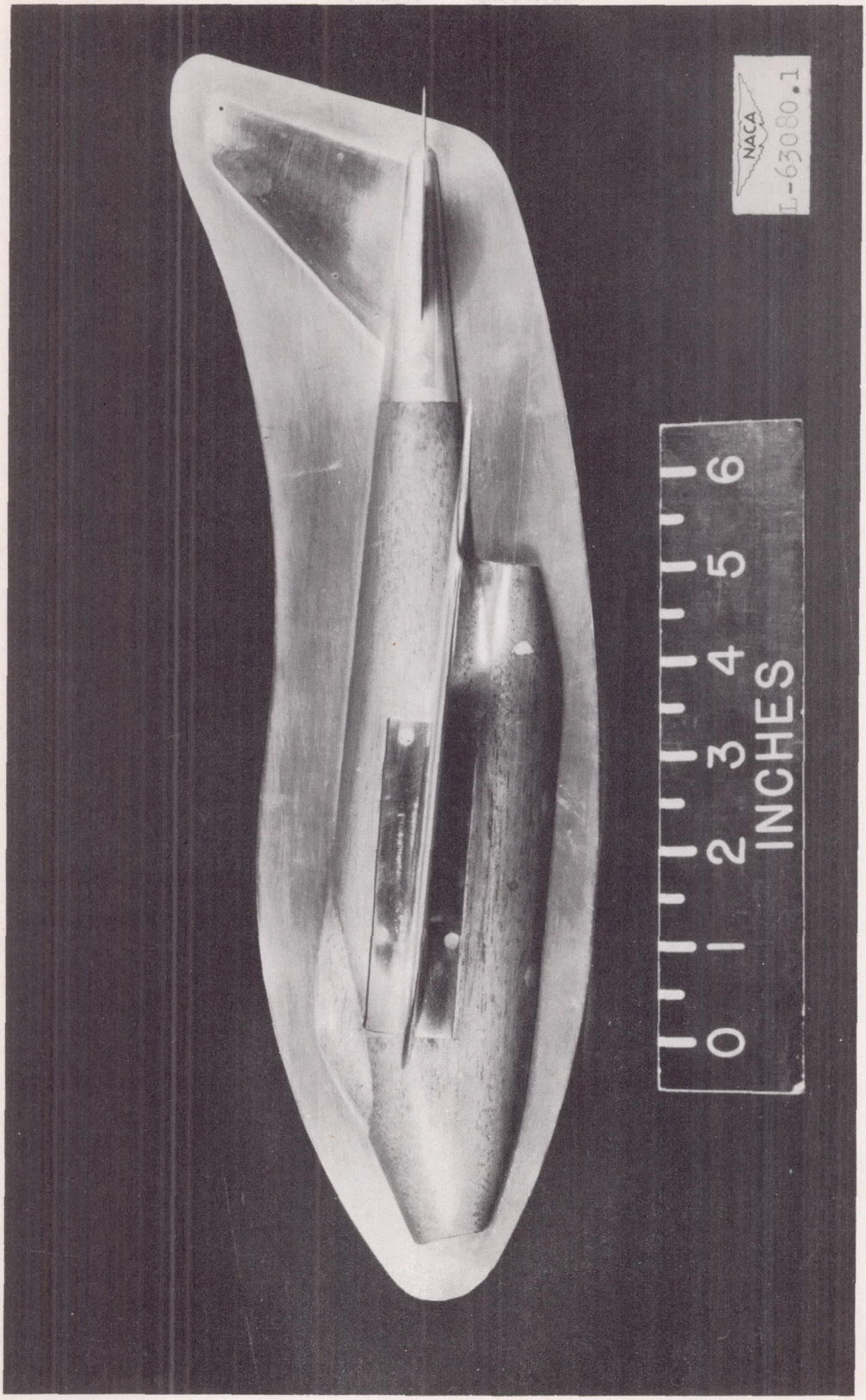


Figure 1.- Side view of semispan wing-flow model of the Bell X-5 airplane.

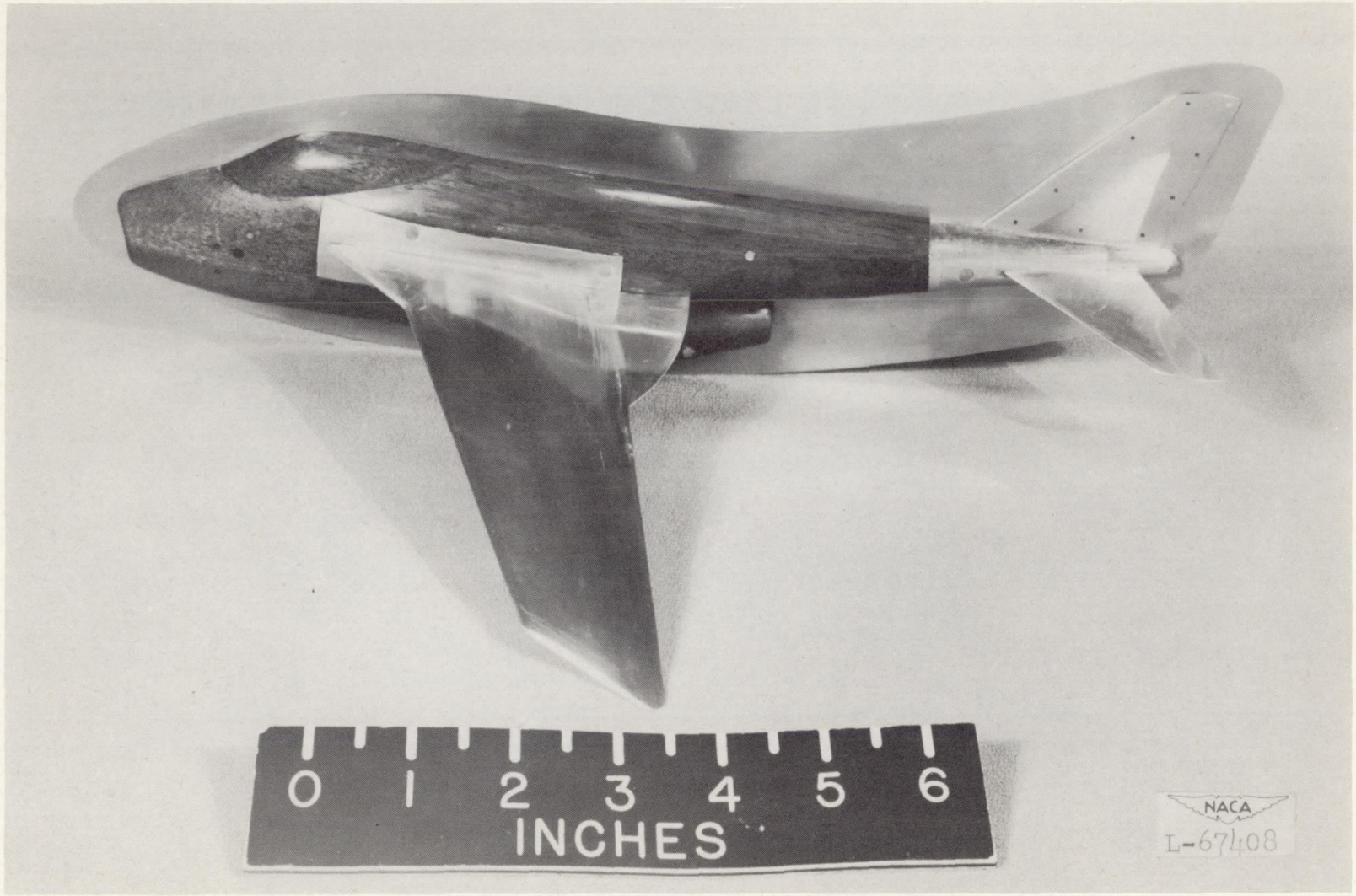


Figure 2.- Semispan wing-flow model of the Bell X-5 variable-sweep airplane. $\Lambda = 20^{\circ}$.

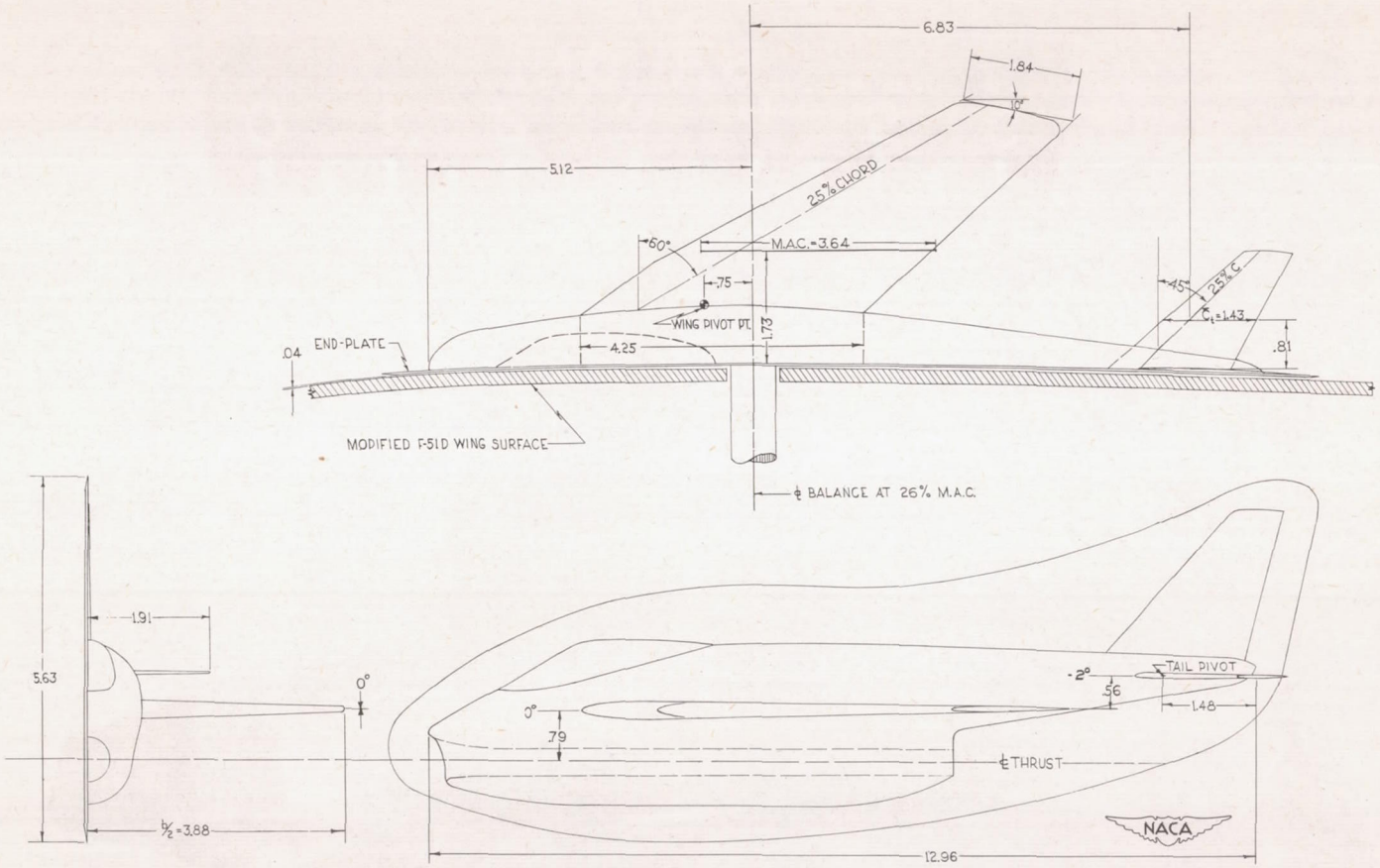


Figure 3.- Details of the semispan model of the Bell X-5 variable-sweep airplane with wing in the 60° sweep position. (All dimensions are in inches.)

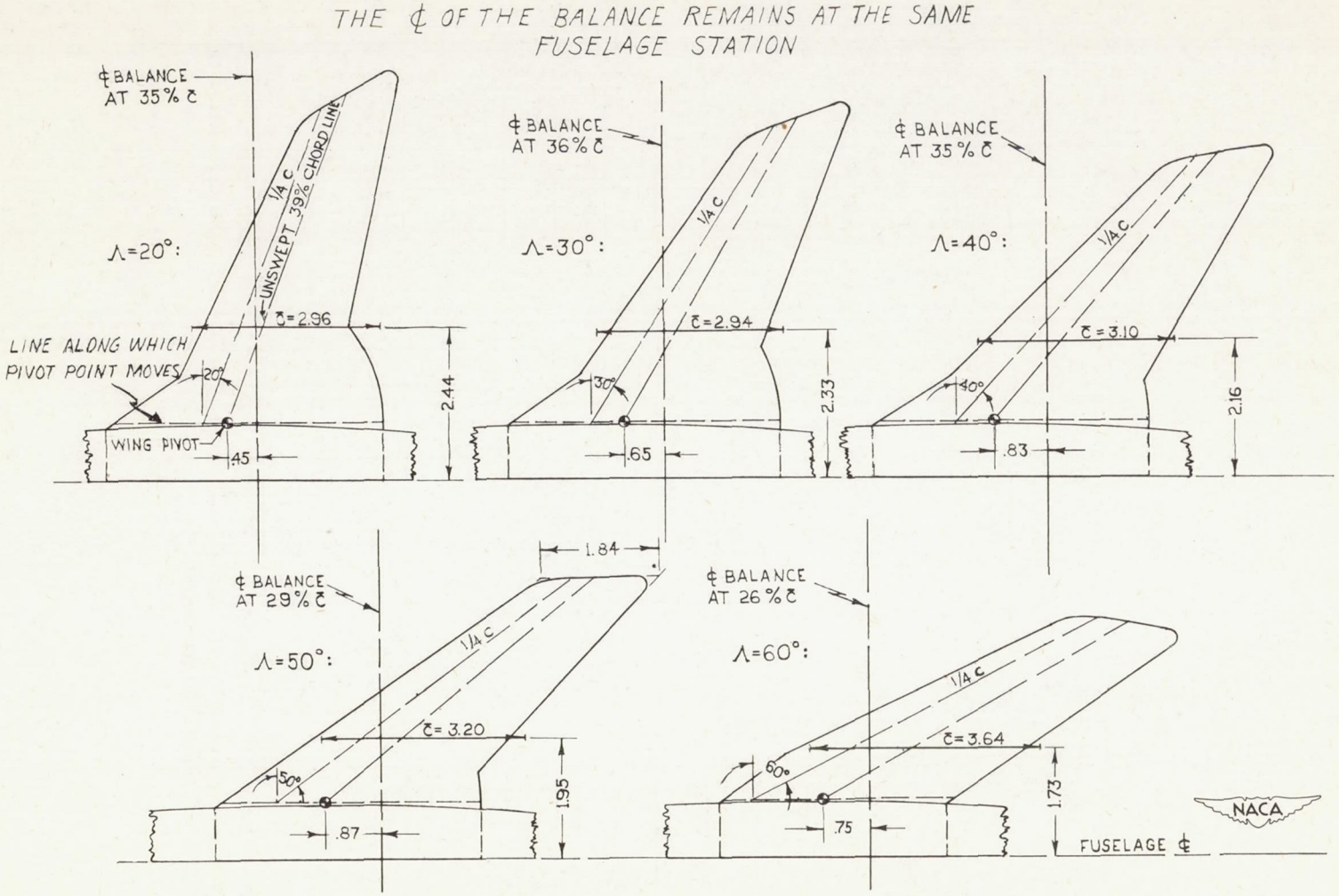


Figure 4.- Various wings of $\frac{1}{30}$ - scale X-5 model. All dimensions are in inches.

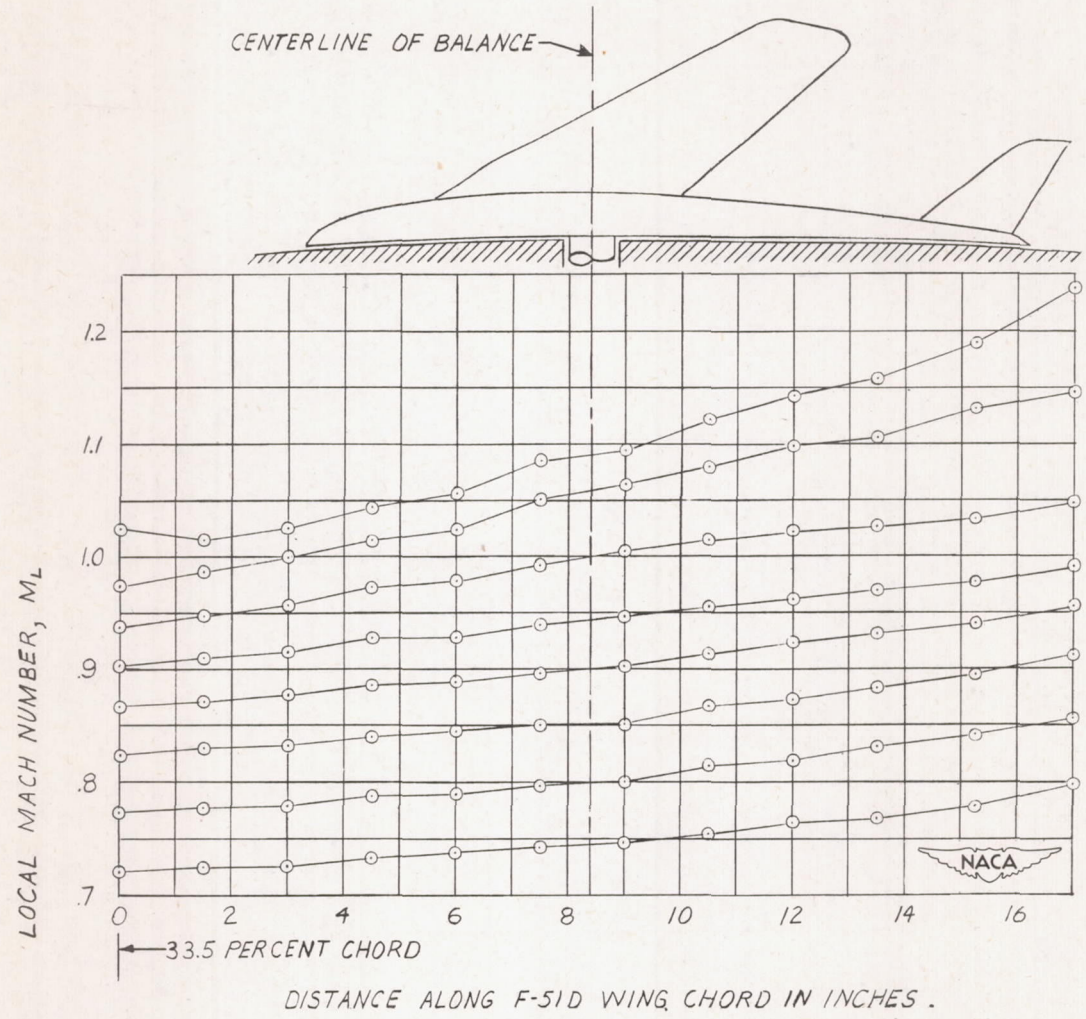


Figure 5.- Typical chordwise local Mach number variation measured at surface of test section for several flight Mach numbers. Chordwise location of model also shown.

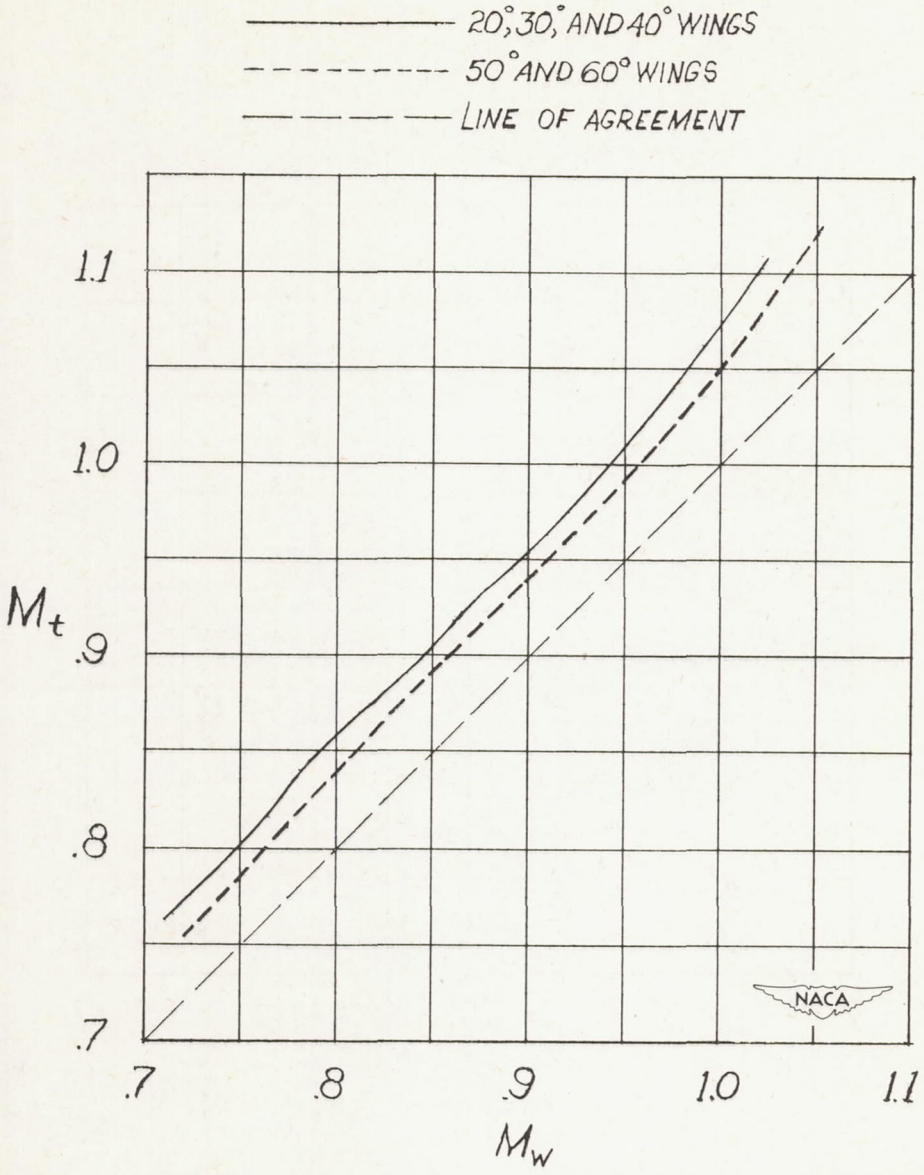


Figure 6.- Variation of Mach number at the tail M_t with Mach number at the various wings M_w. Line of agreement also shown.

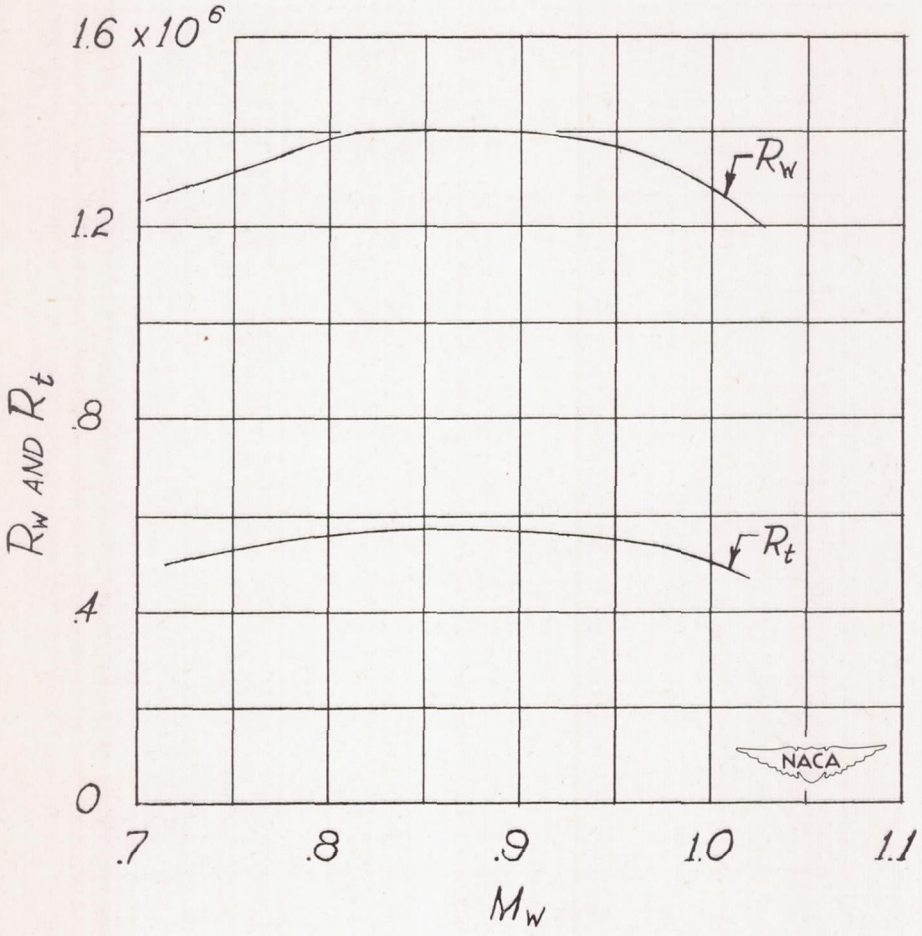


Figure 7.- Variation of Reynolds number of wing ($\Lambda = 60^\circ$) R_W and Reynolds number of tail R_T with Mach number at the wing M_W.

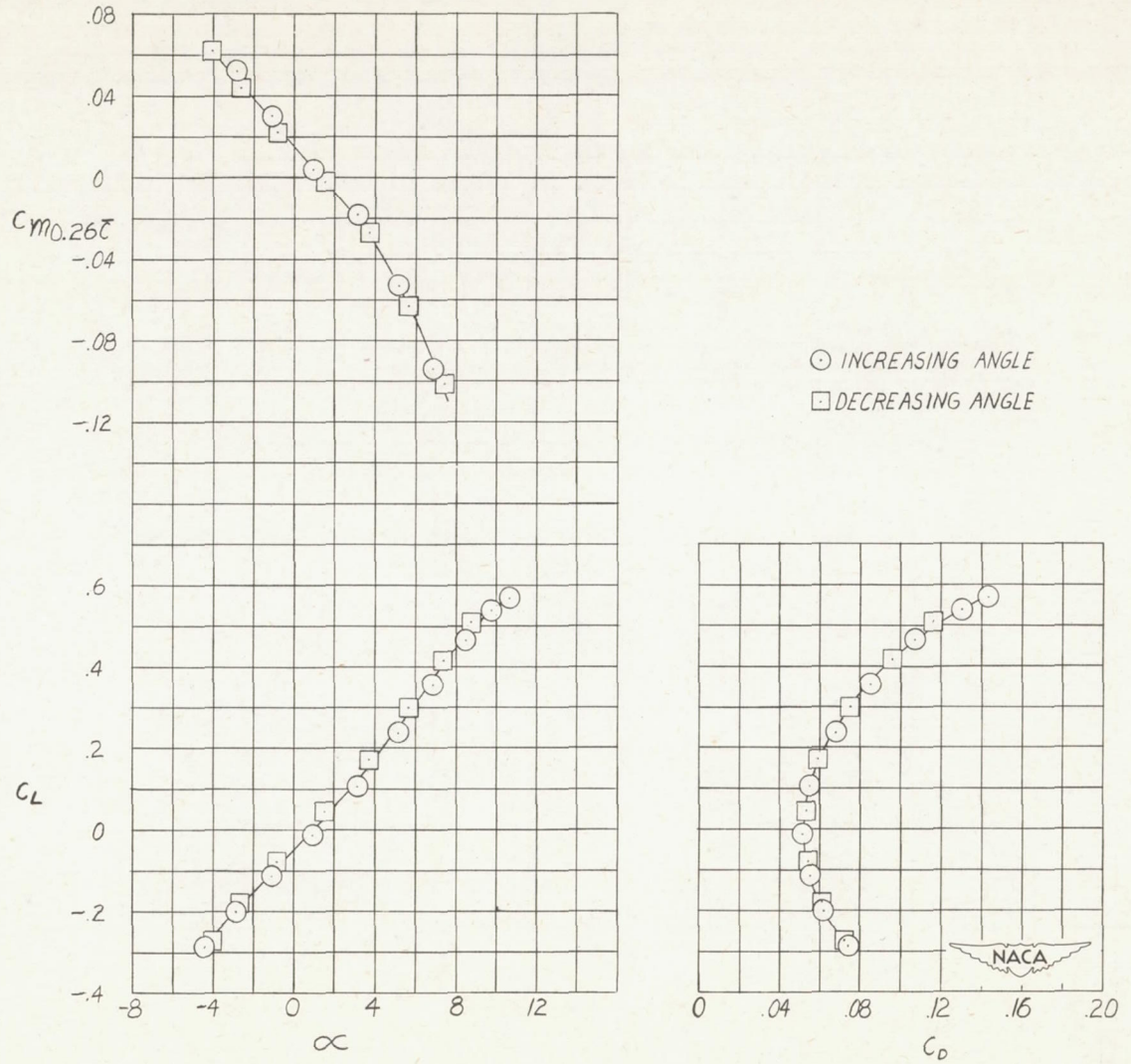
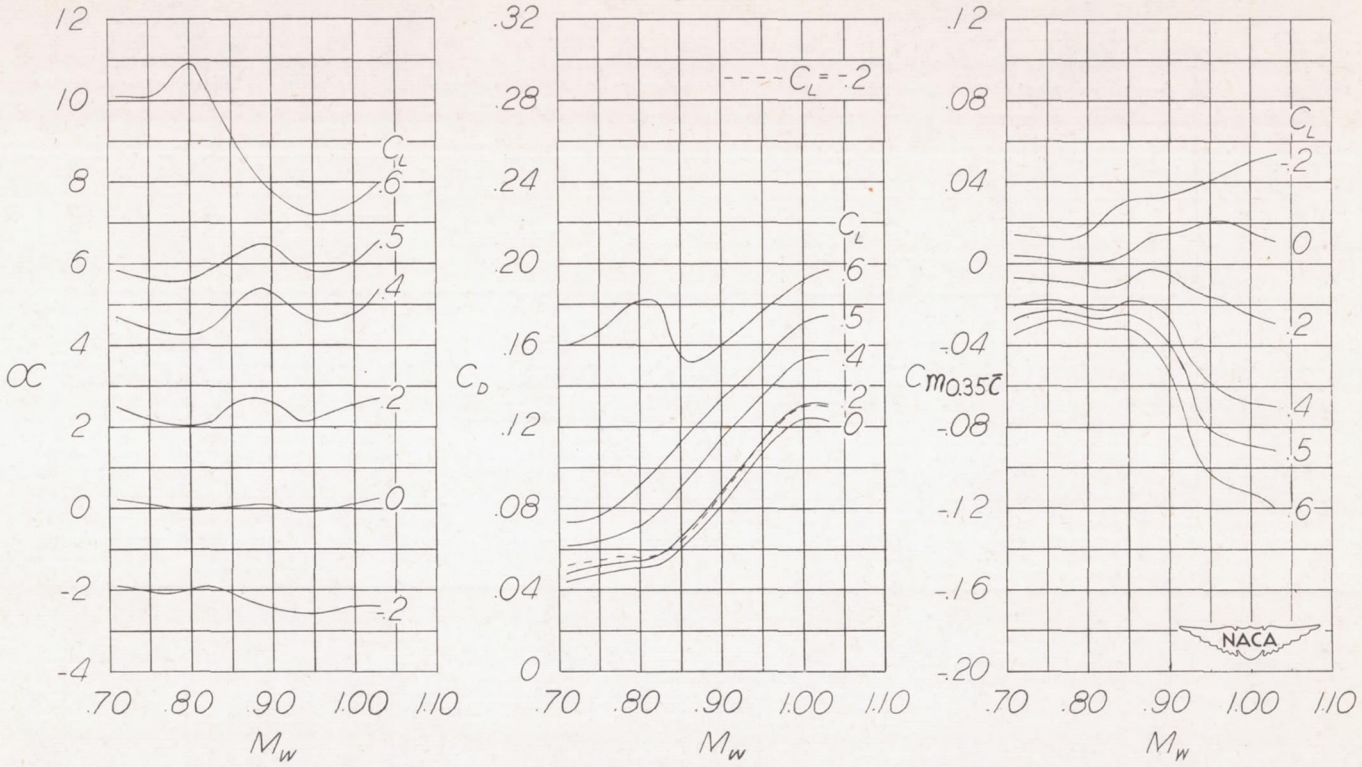


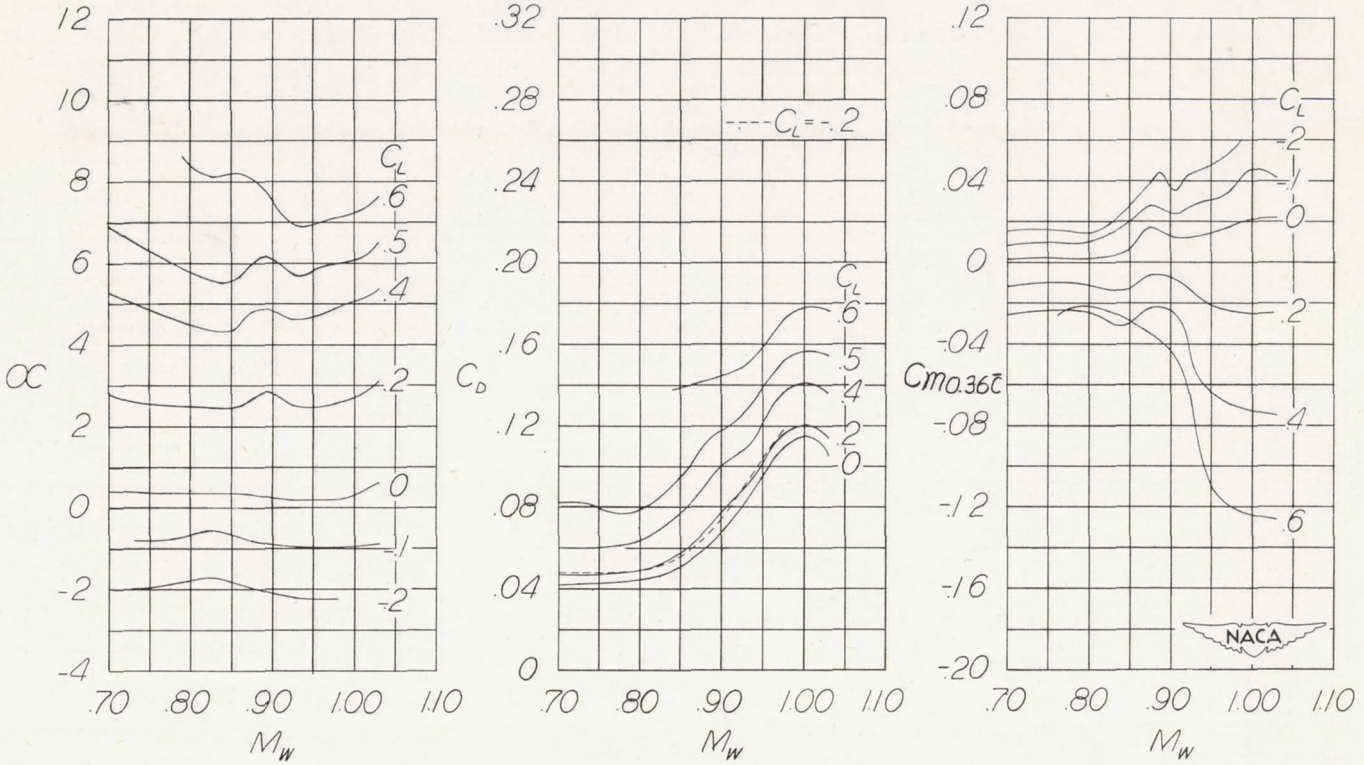
Figure 8.- Sample data of semispan model of Bell X-5 airplane. $\Lambda = 60^{\circ}$; $M_W = 0.90$; $i_t = -2^{\circ}$.

CONFIDENTIAL



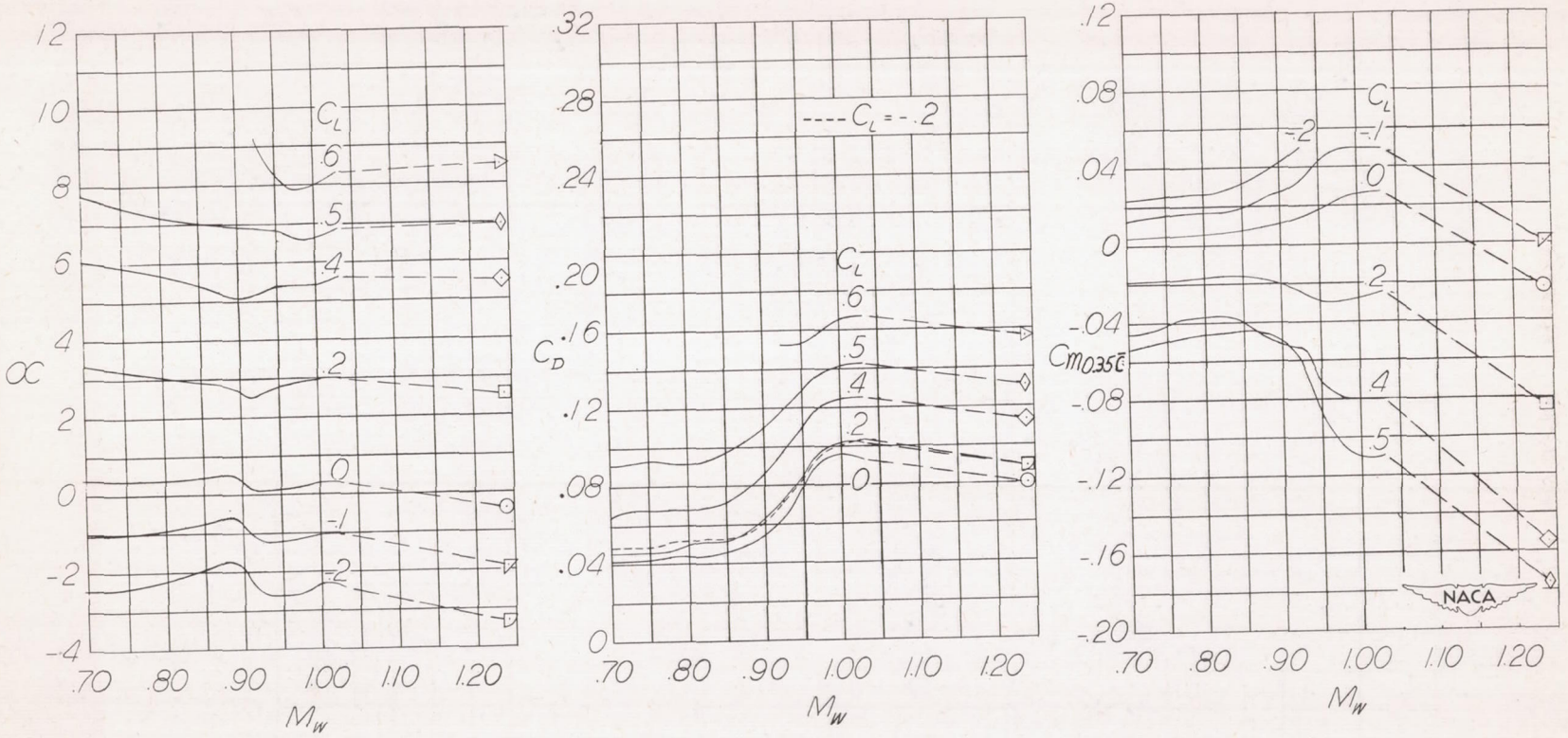
(a) $\Lambda = 20^\circ$.

Figure 9.- Variation of angle of attack, drag coefficient, and pitching-moment coefficient with Mach number at several values of lift coefficient of a semispan model of the Bell X-5; $i_t = -2^\circ$.



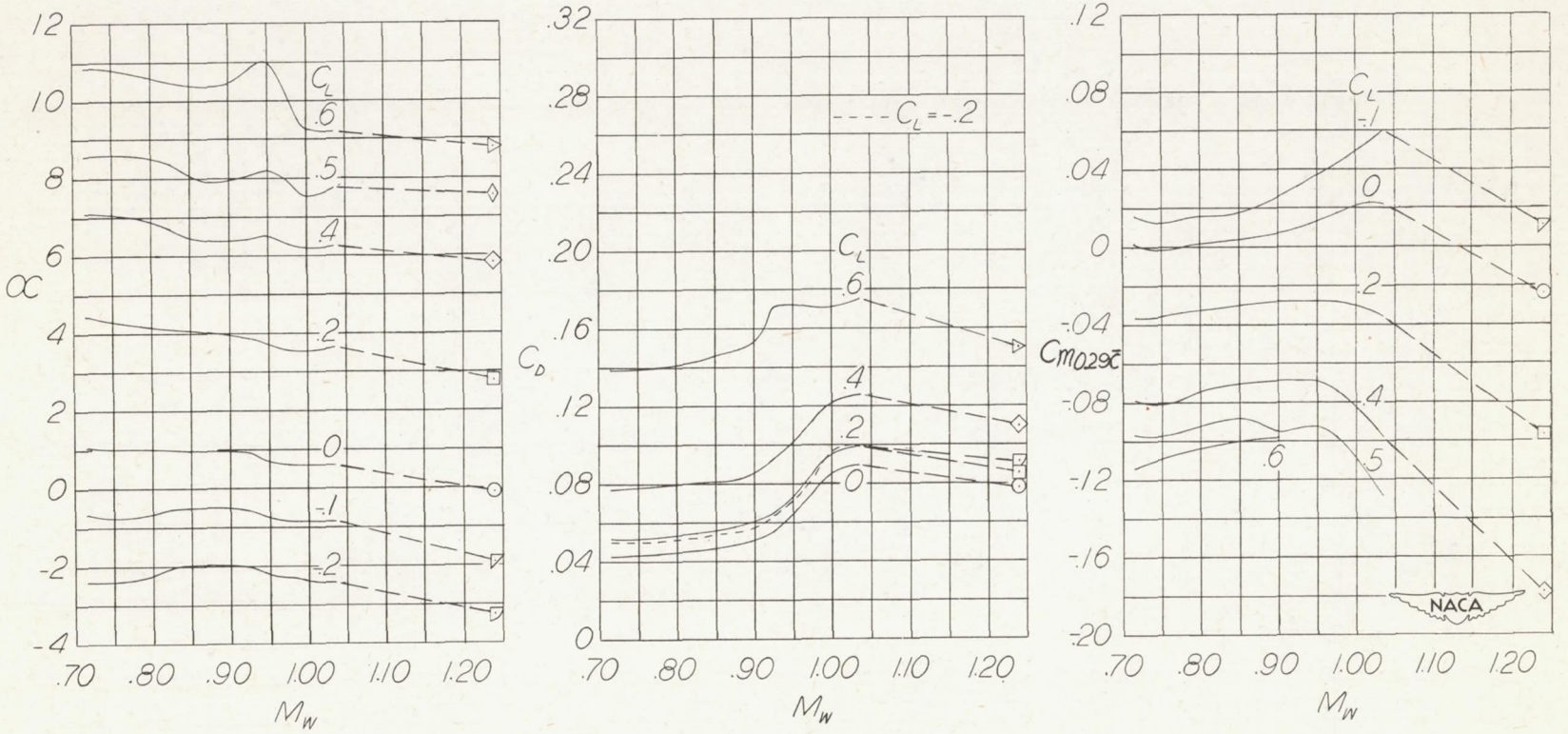
(b) $\Lambda = 30^\circ$.

Figure 9.- Continued.



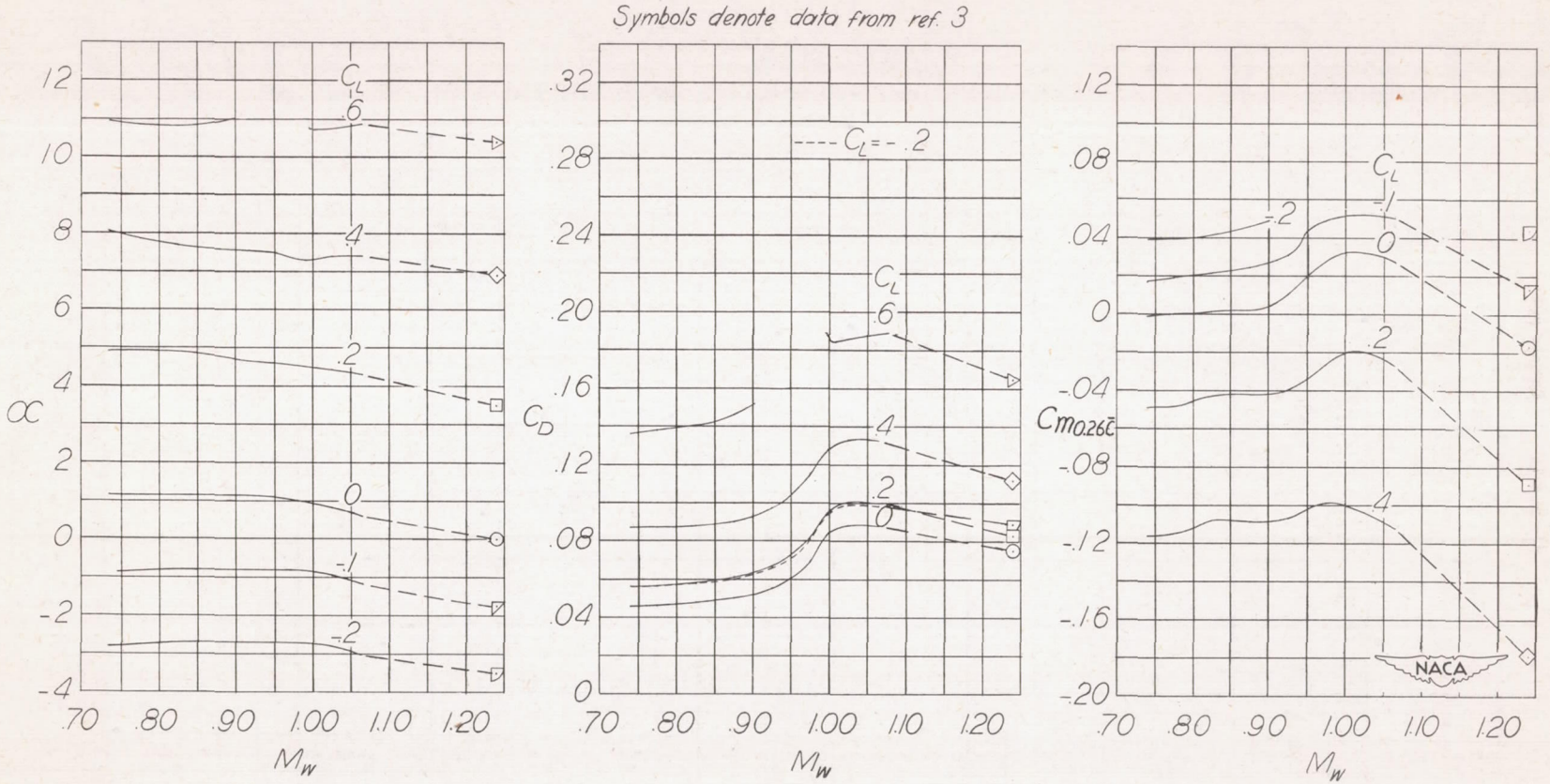
(c) $\Lambda = 40^\circ$.

Figure 9.- Continued.



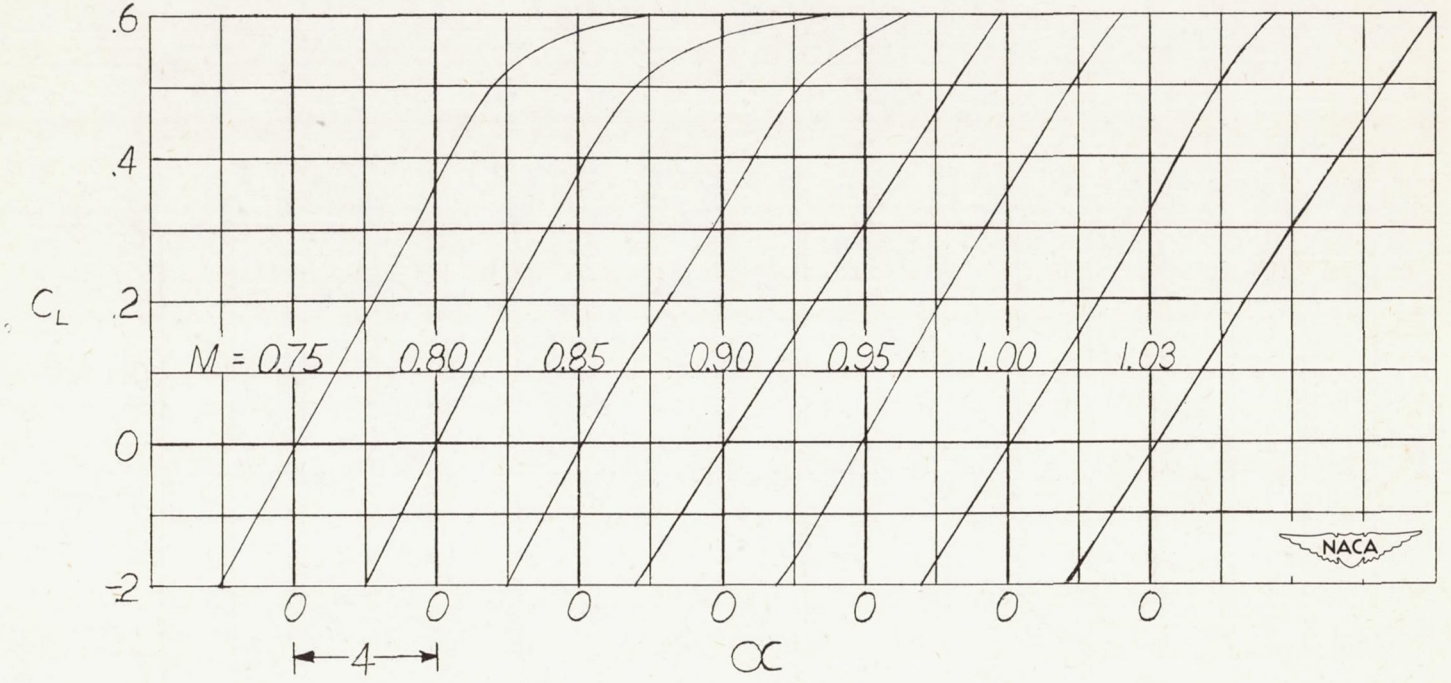
(d) $\Lambda = 50^\circ$.

Figure 9.- Continued.



(e) $\Lambda = 60^\circ$.

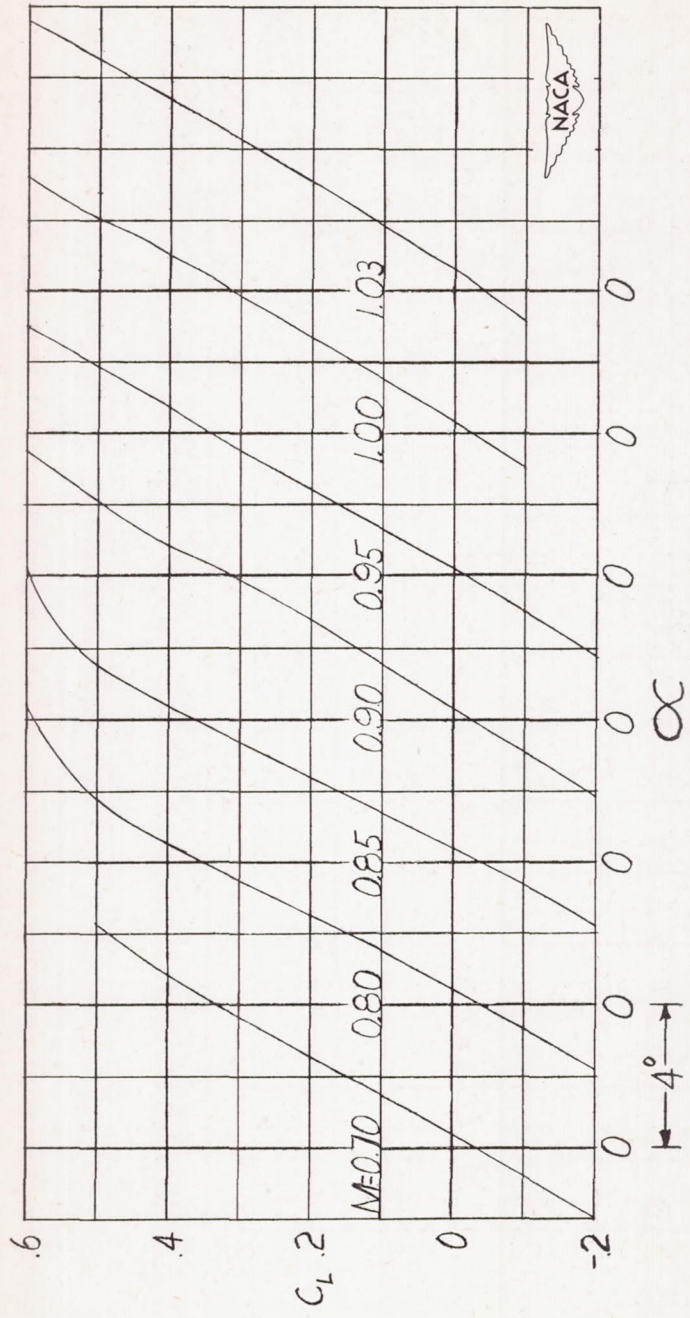
Figure 9.- Concluded.



(a) $\Lambda = 20^{\circ}$.

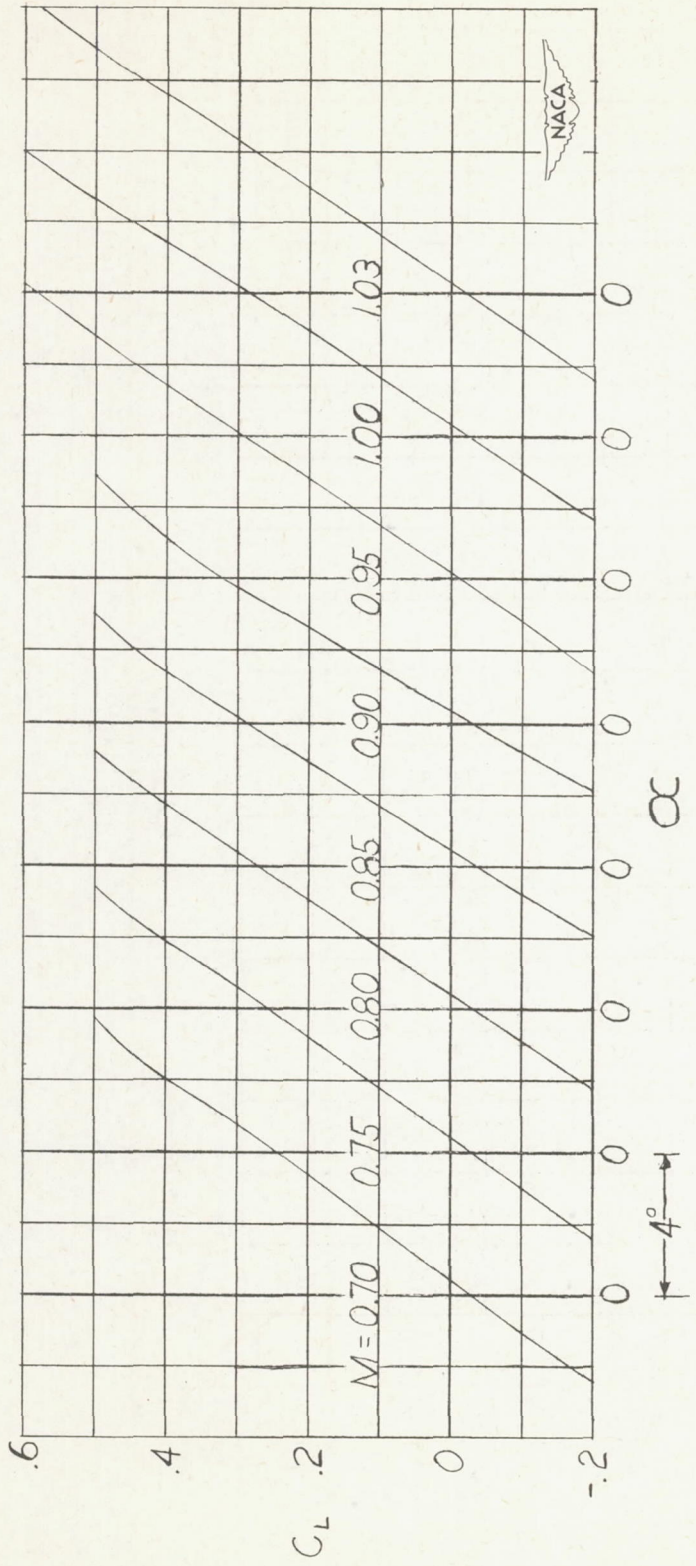
Figure 10.- Variation of lift coefficient with angle of attack at several Mach numbers.

CONFIDENTIAL



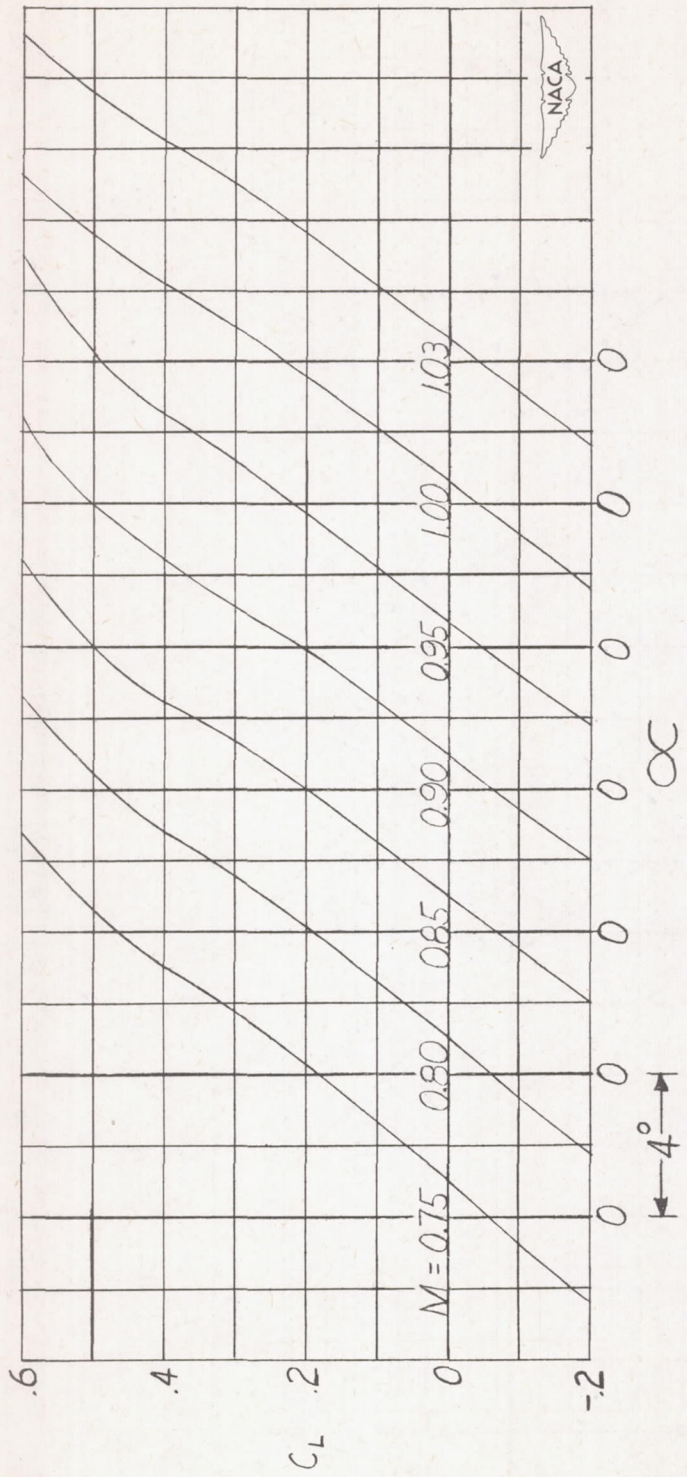
(b) $\Lambda = 30°$.

Figure 10.- Continued.



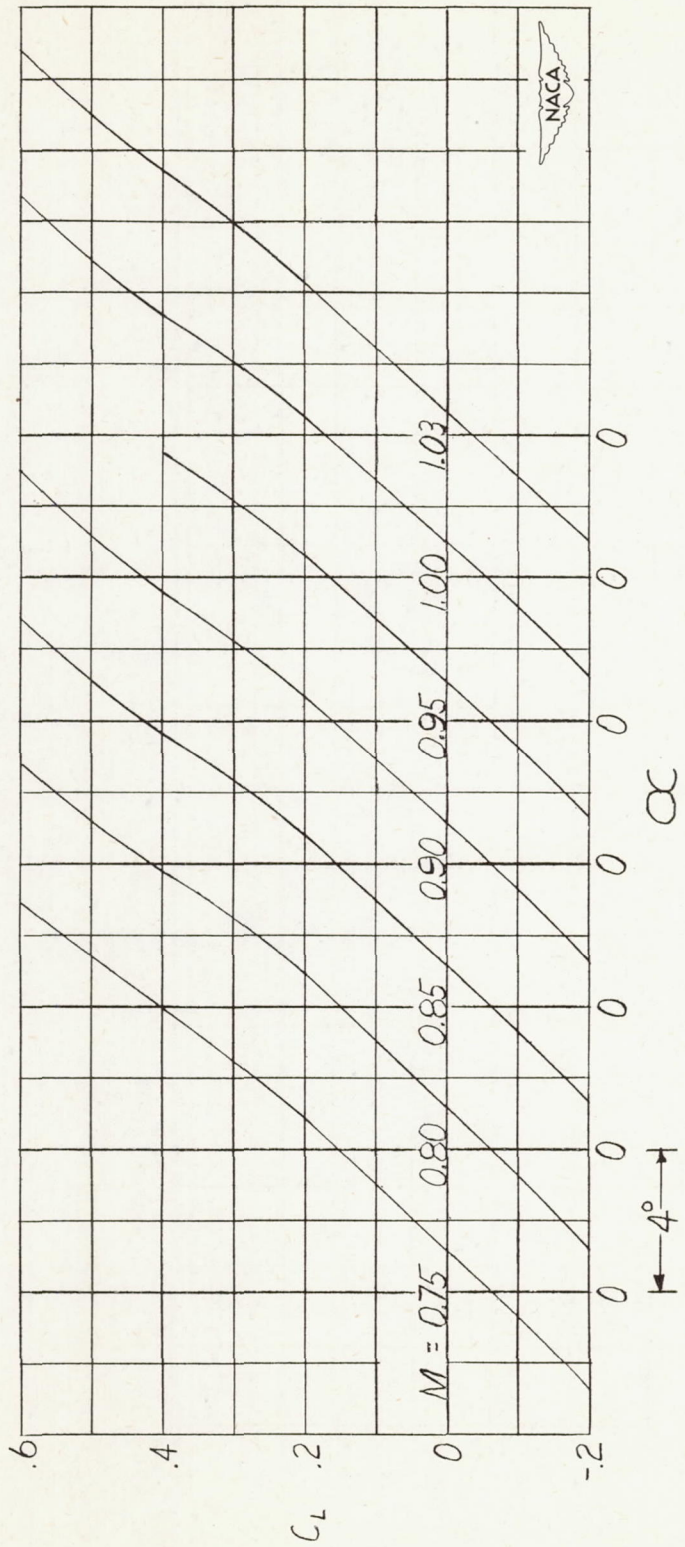
(c) $\Lambda = 40°$.

Figure 10.- Continued.



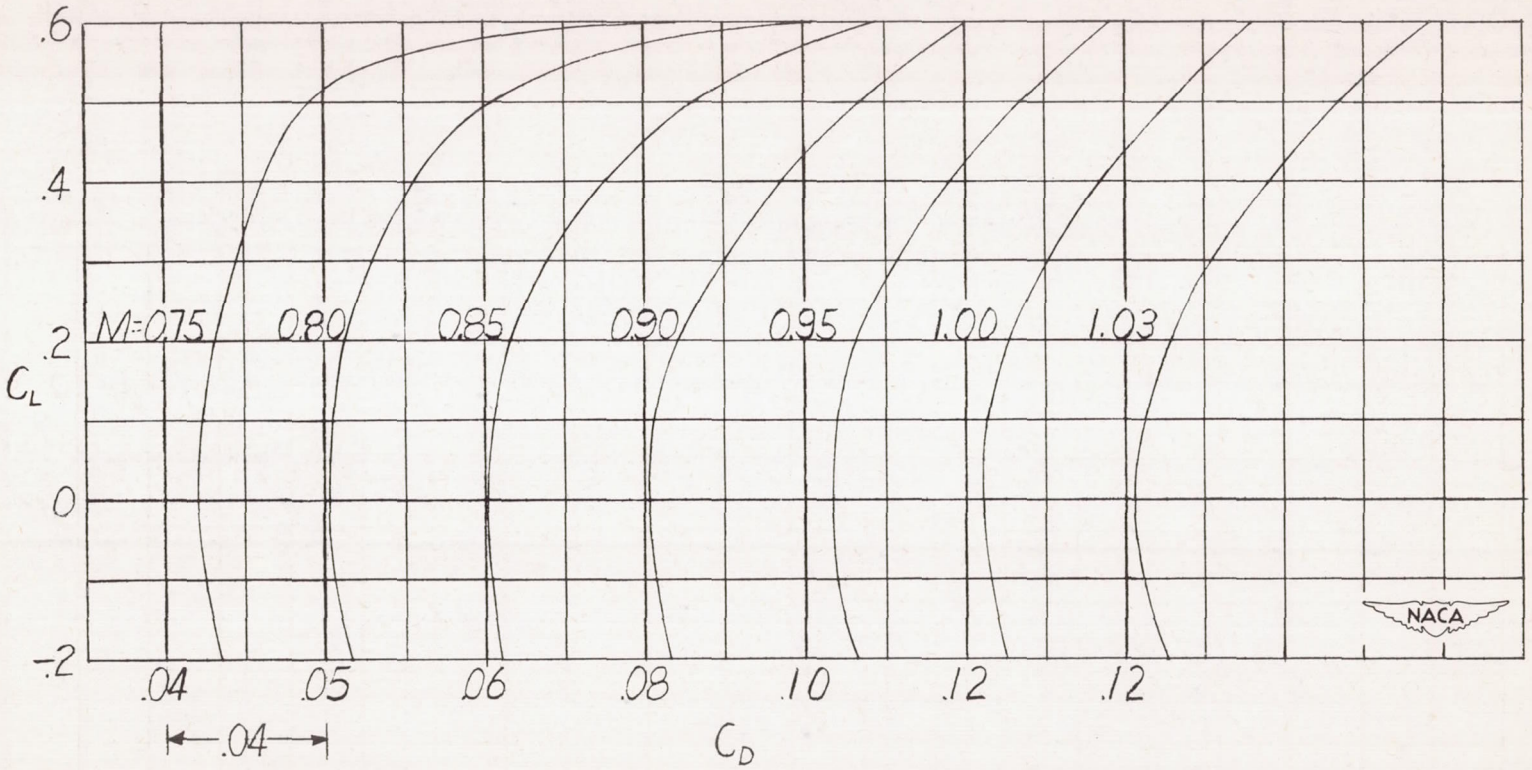
(d) $\Lambda = 50°$.

Figure 10.- Continued.



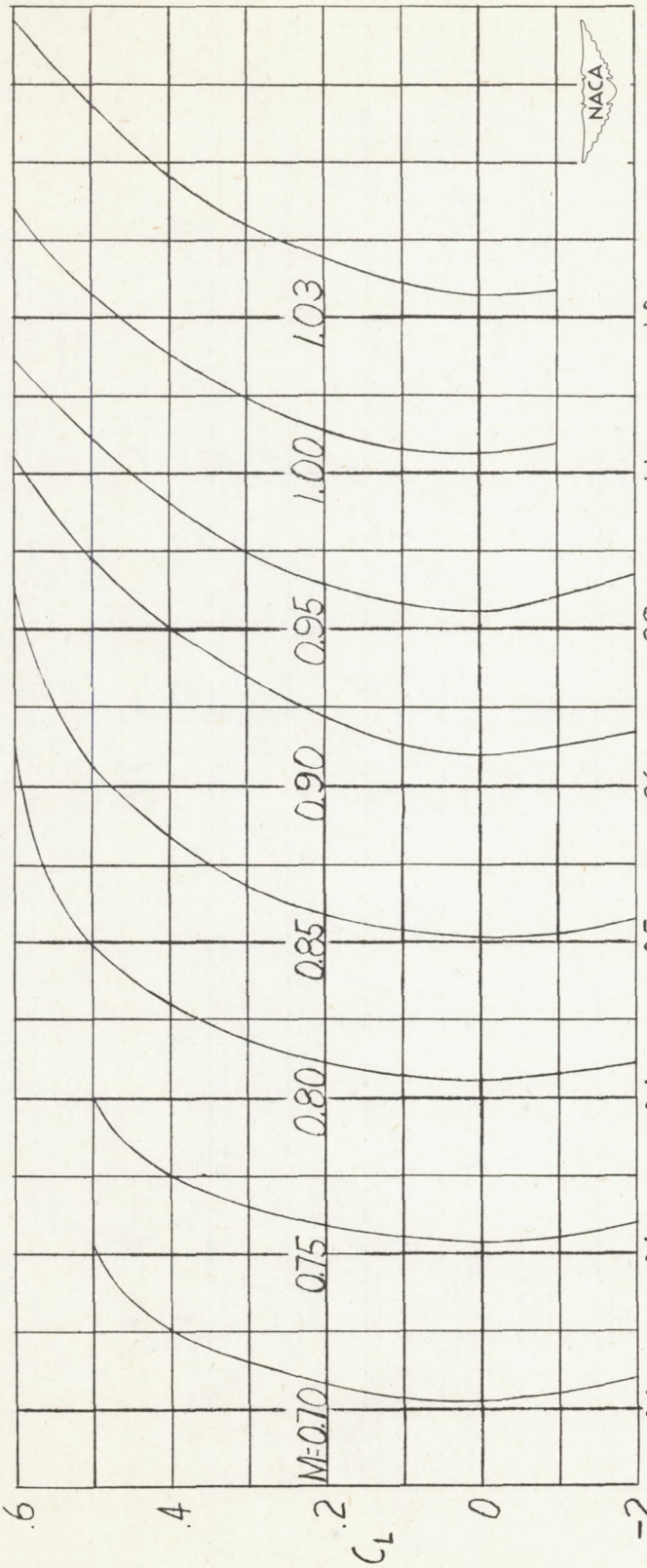
(e) $\Lambda = 60°$.

Figure 10.- Concluded.



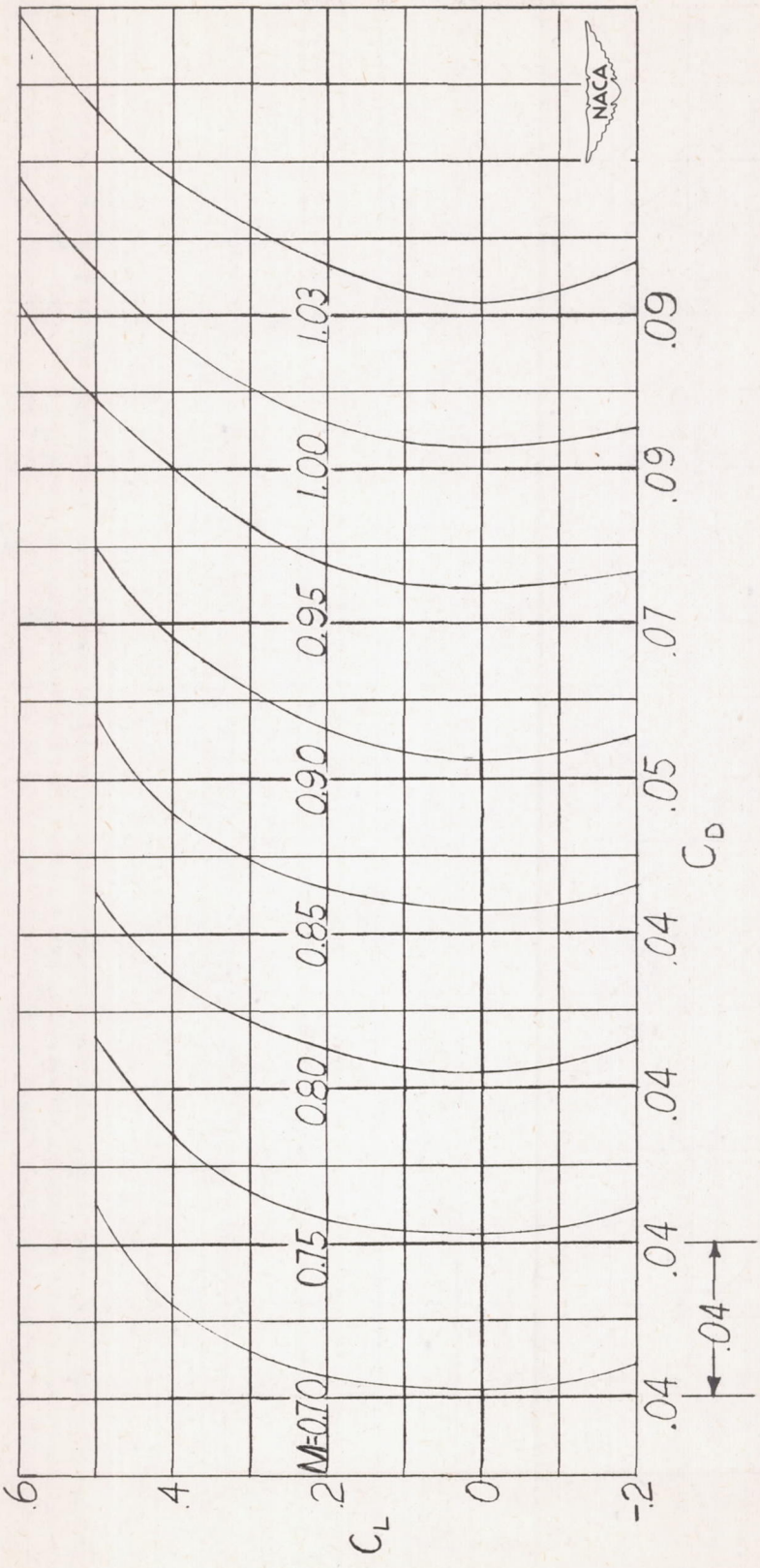
(a) $\Lambda = 20°$.

Figure 11.- Variation of lift coefficient with drag coefficient at several Mach numbers.



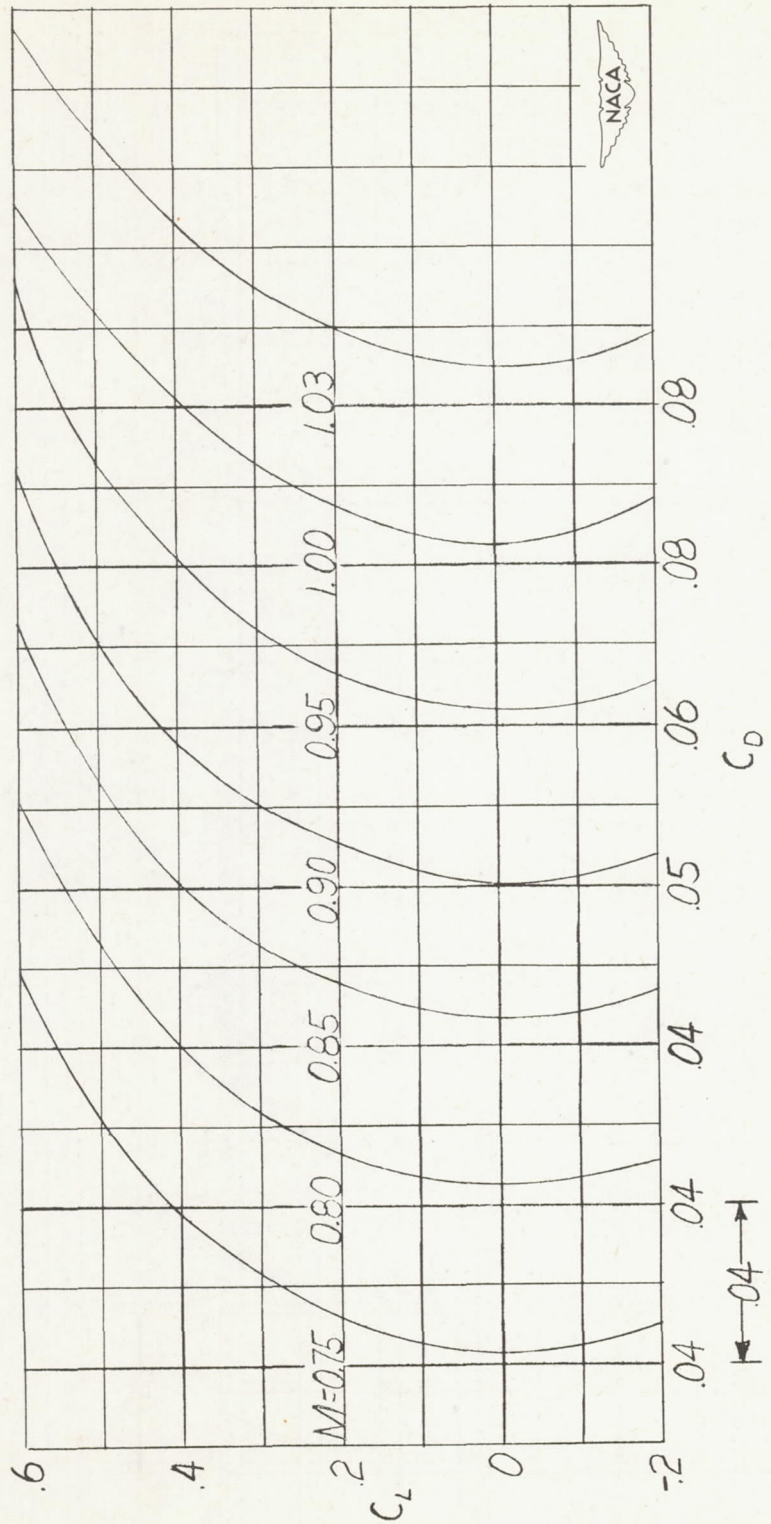
(b) $\Lambda = 30^{\circ}$.

Figure 11.- Continued.



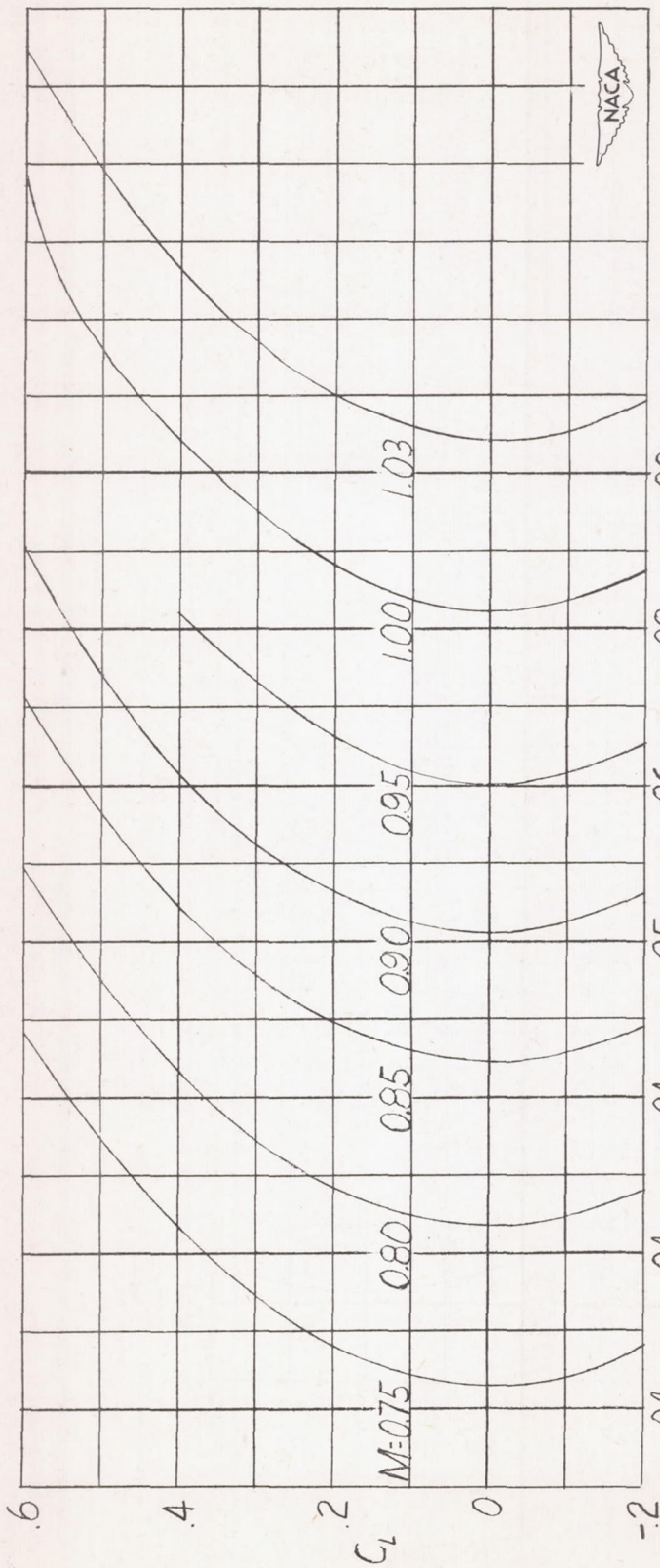
(c) $\Lambda = 40°$.

Figure 11.- Continued.



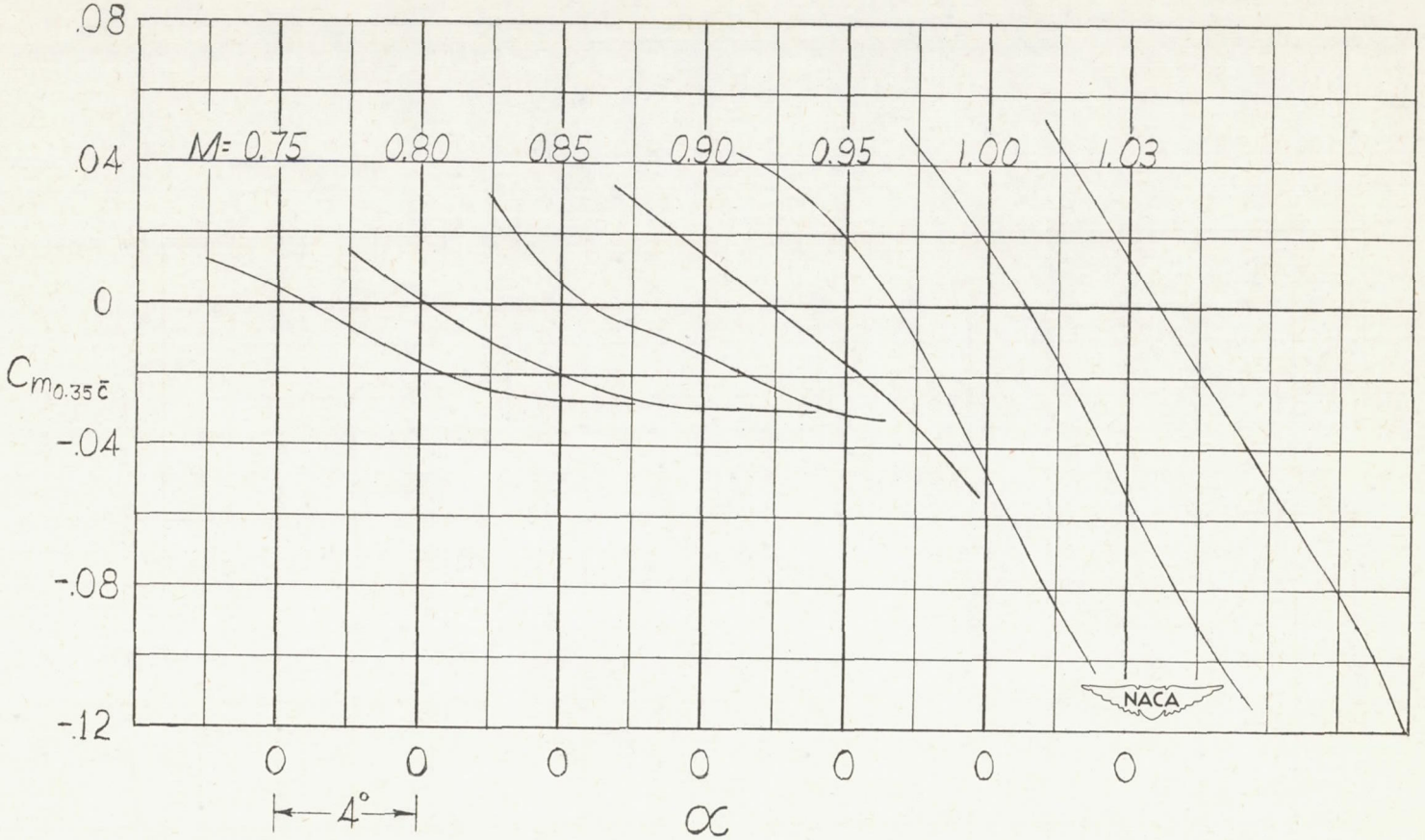
(d) $\Lambda = 50°$.

Figure 11.- Continued.



(e) $\Lambda = 60°$.

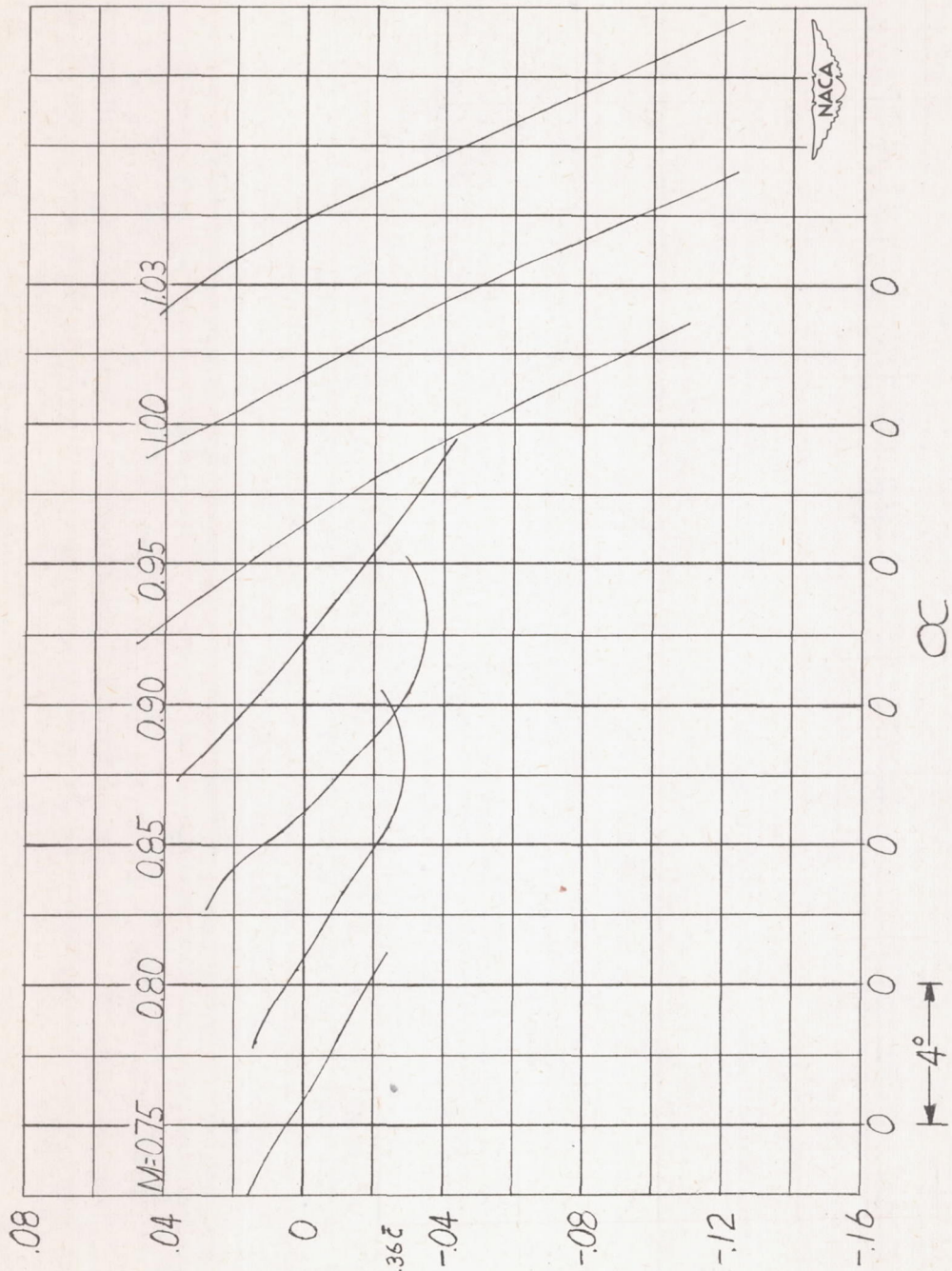
Figure 11.- Concluded.



(a) $\Lambda = 20^{\circ}$.

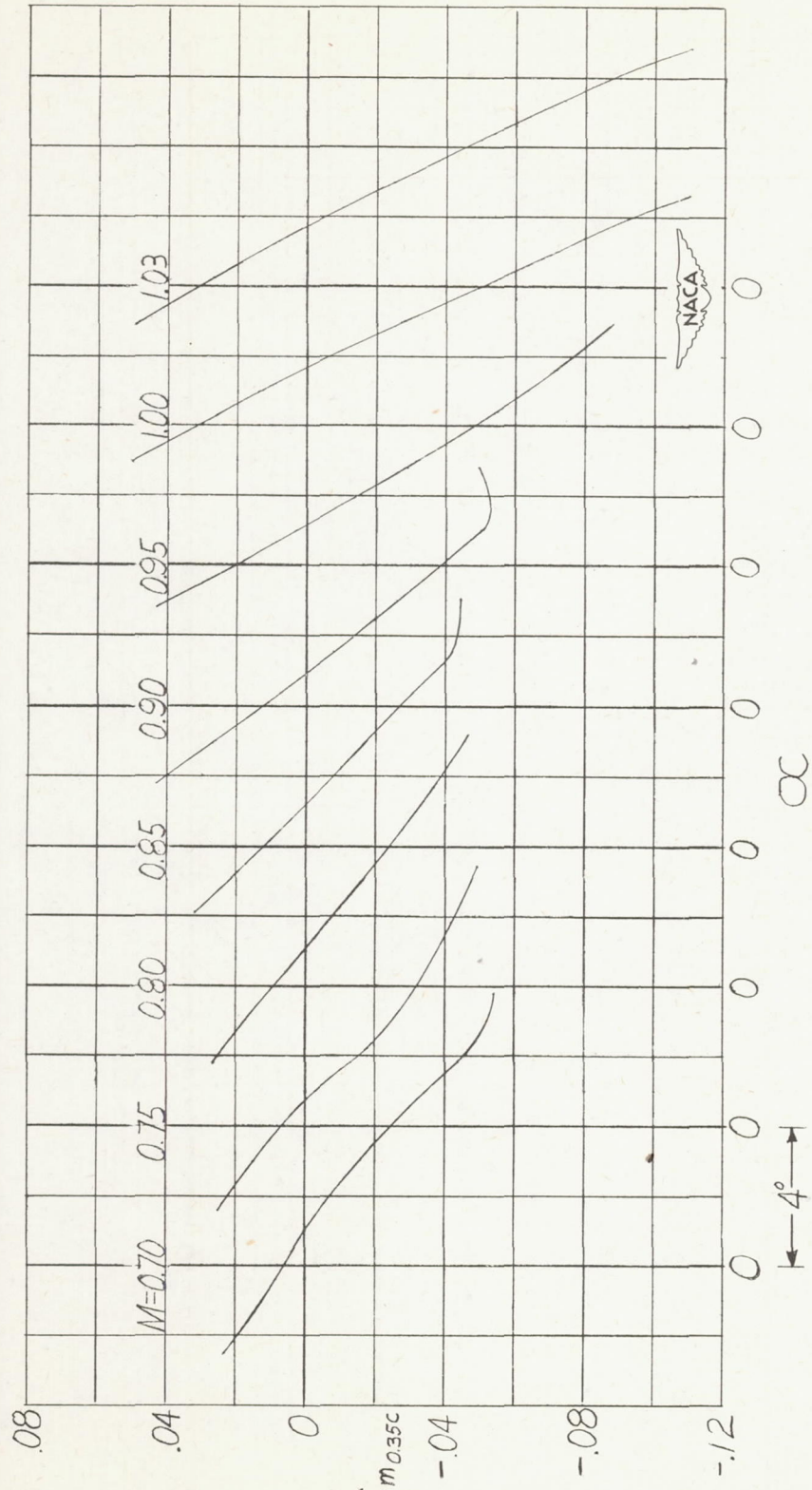
Figure 12.- Variation of pitching-moment coefficient with angle of attack at several Mach numbers.

CONFIDENTIAL



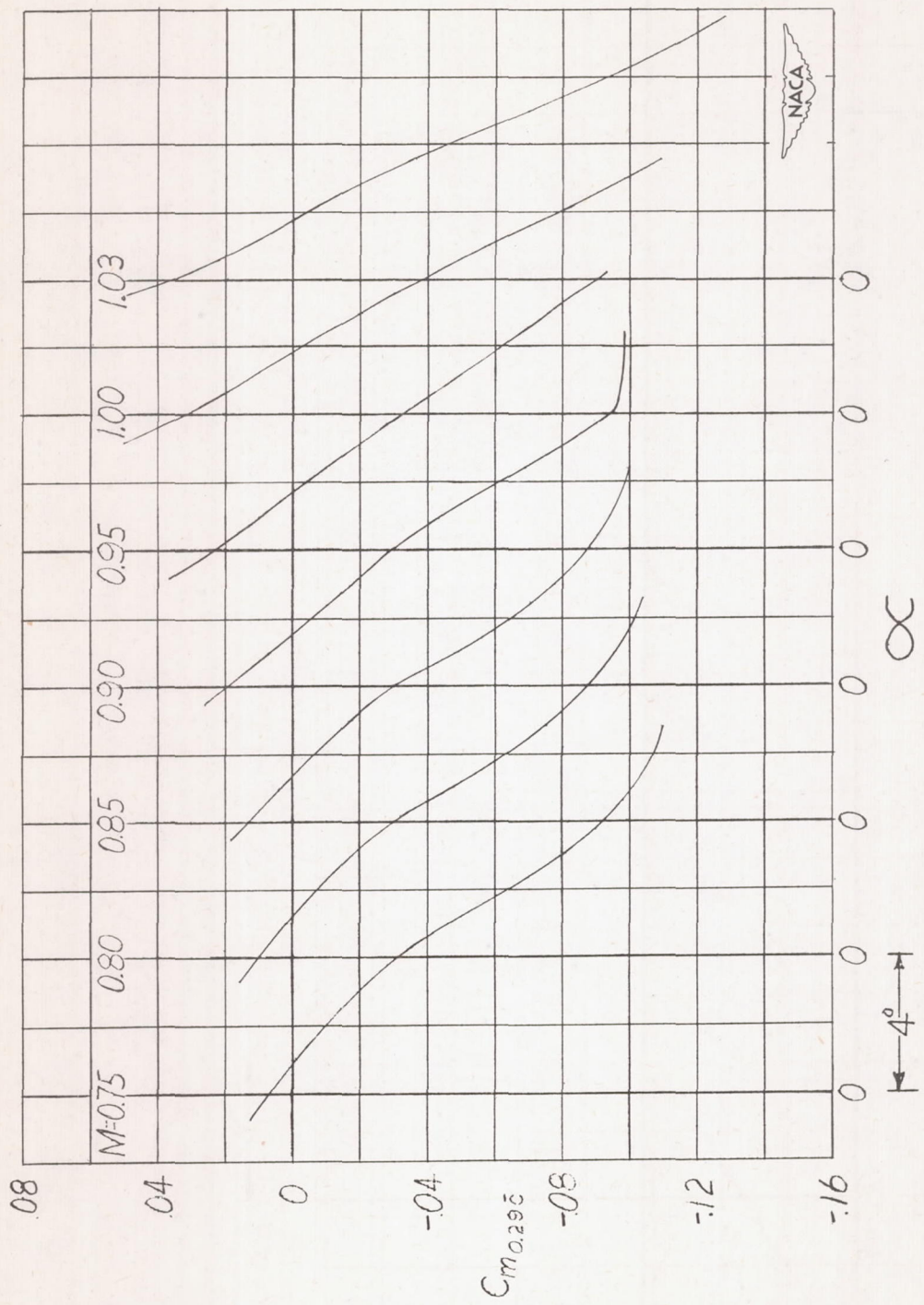
(b) $\Lambda = 30°$.

Figure 12.- Continued.



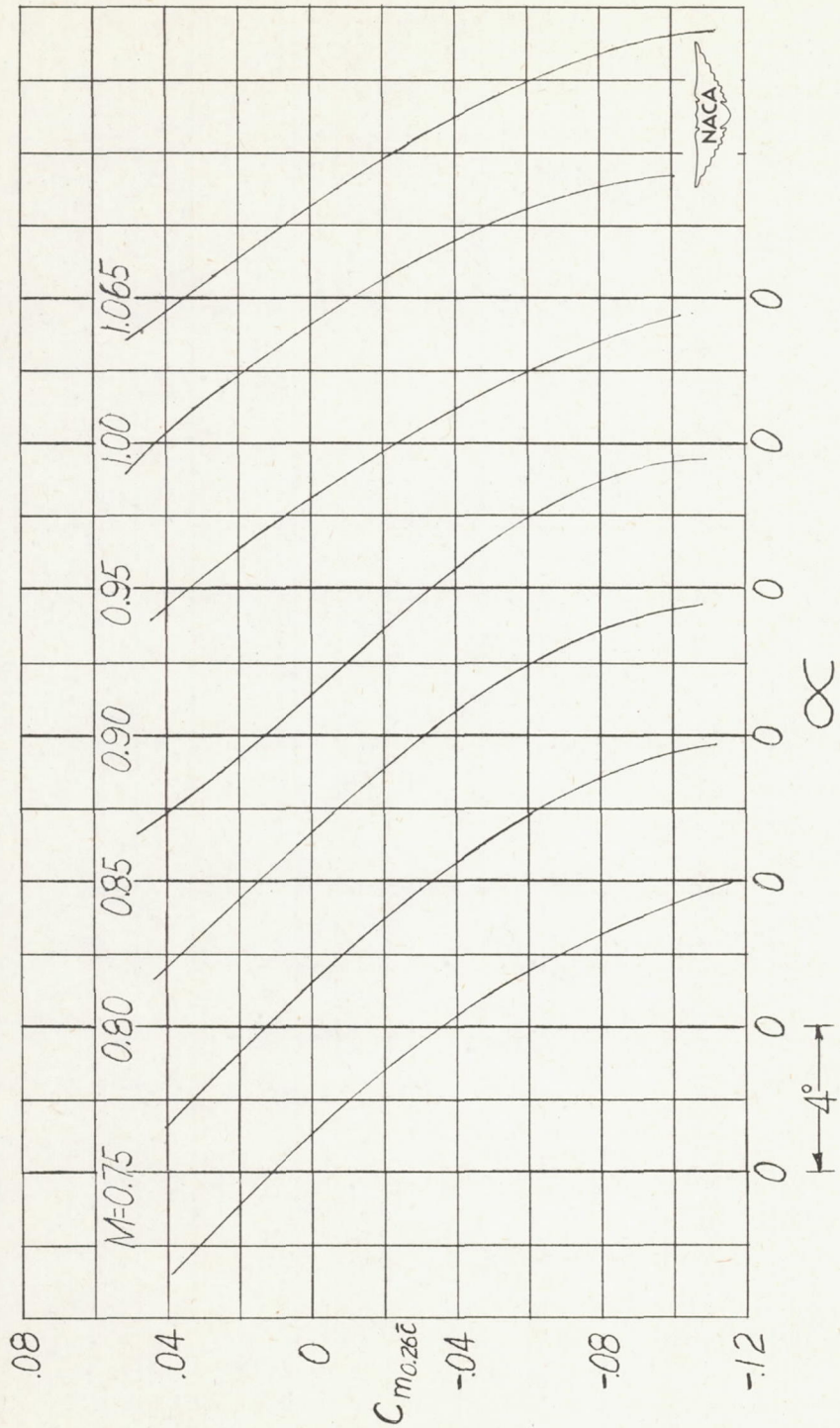
(c) $\Lambda = 40°$.

Figure 12.- Continued.



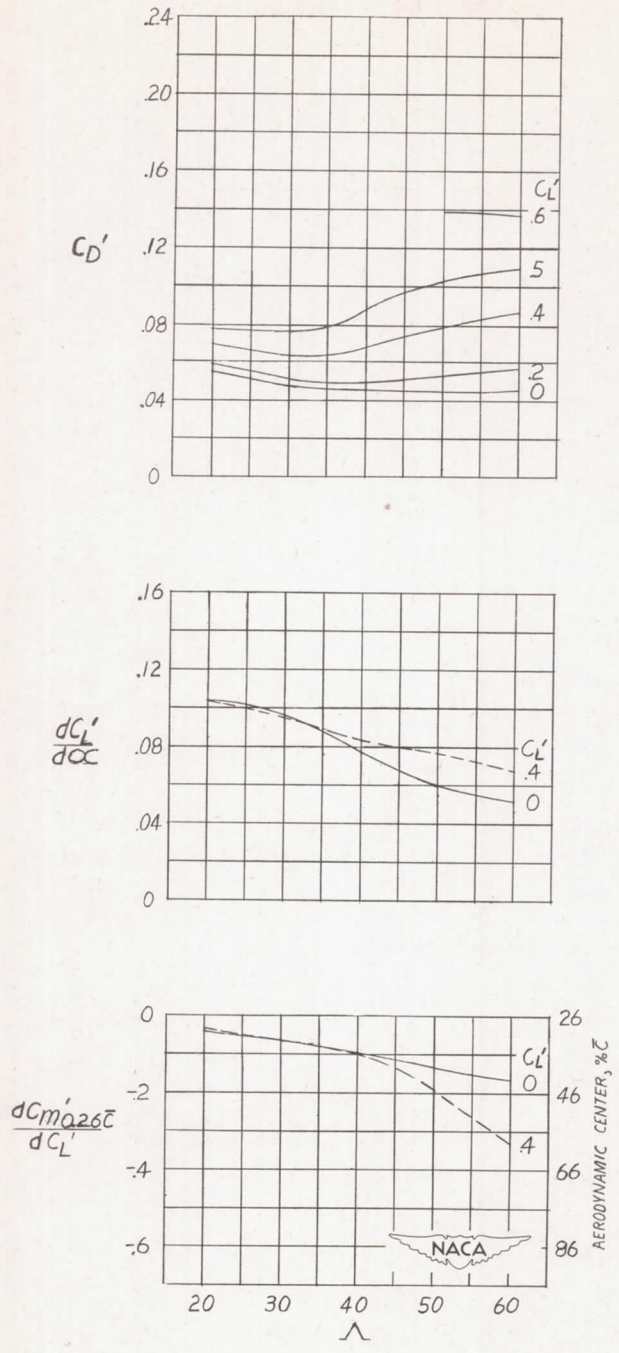
(d) $\Lambda = 50°$.

Figure 12.- Continued.



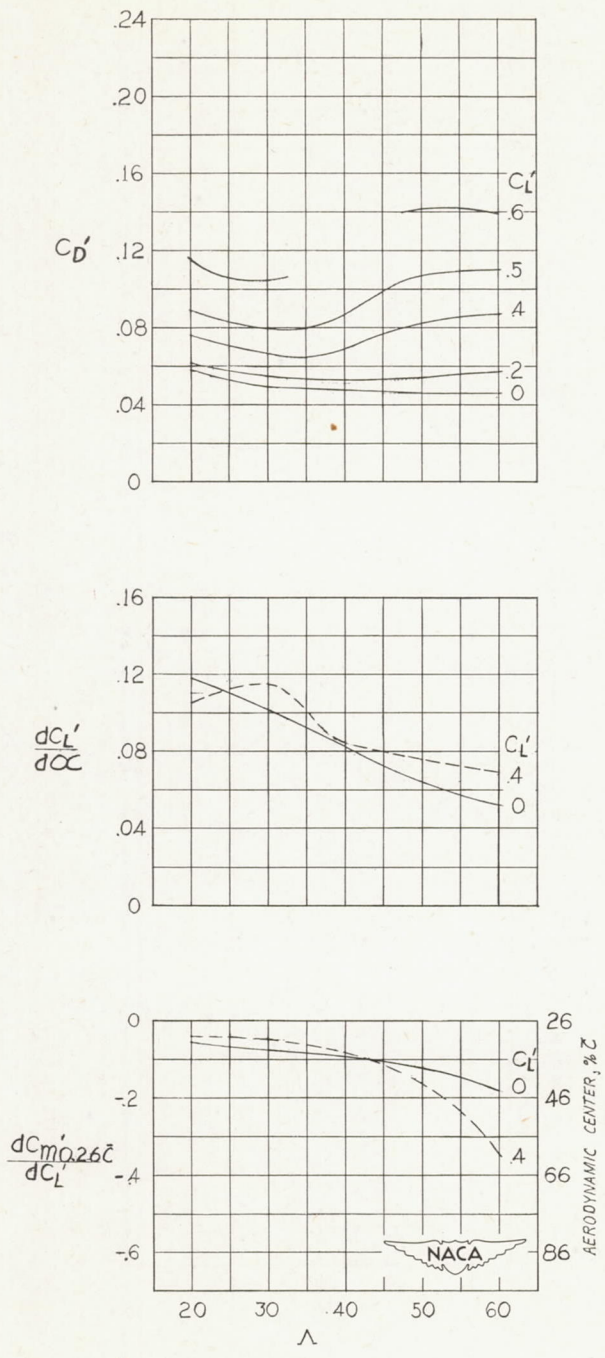
(e) $\Lambda = 60°$.

Figure 12.- Concluded.



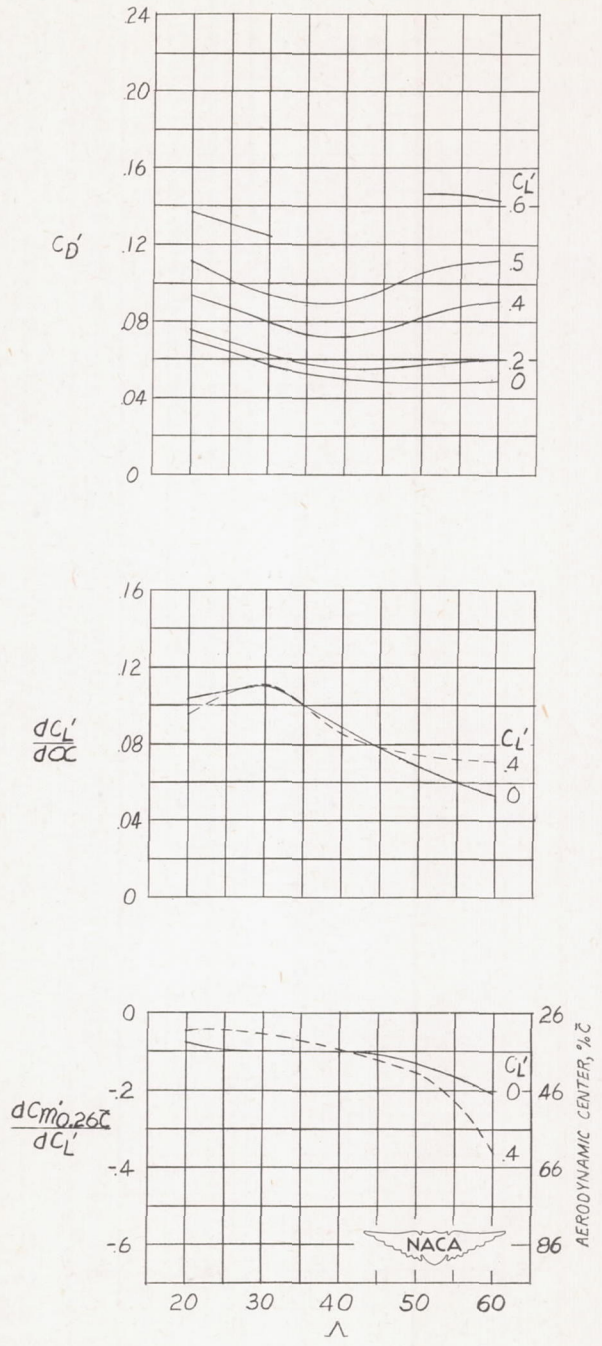
(a) M = 0.75.

Figure 13.- Effect of sweepback angle on the drag coefficient at various lift coefficients, on the rate of change of lift coefficient with angle of attack, and on the rate of change of pitching-moment coefficient with lift coefficient for the semispan model of the Bell X-5 airplane. $i_t = -2^\circ$. (All coefficients based on dimensions of the 60° wing.)



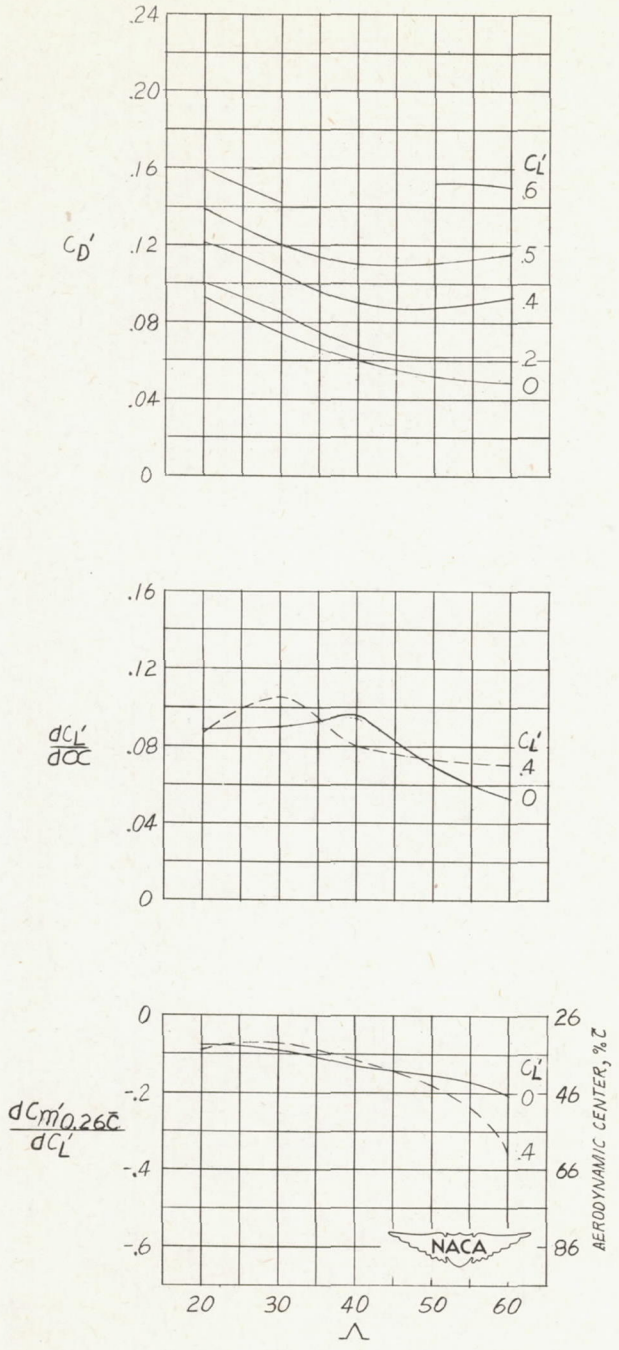
(b) M = 0.80.

Figure 13.- Continued.



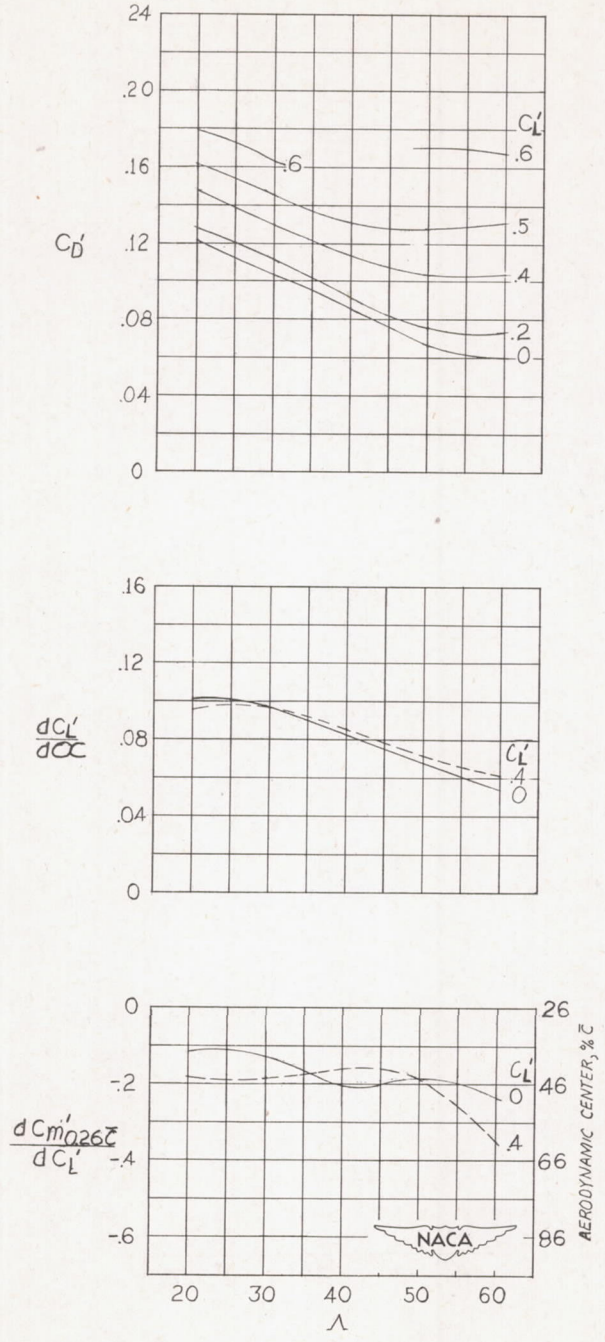
(c) M = 0.85.

Figure 13.- Continued.



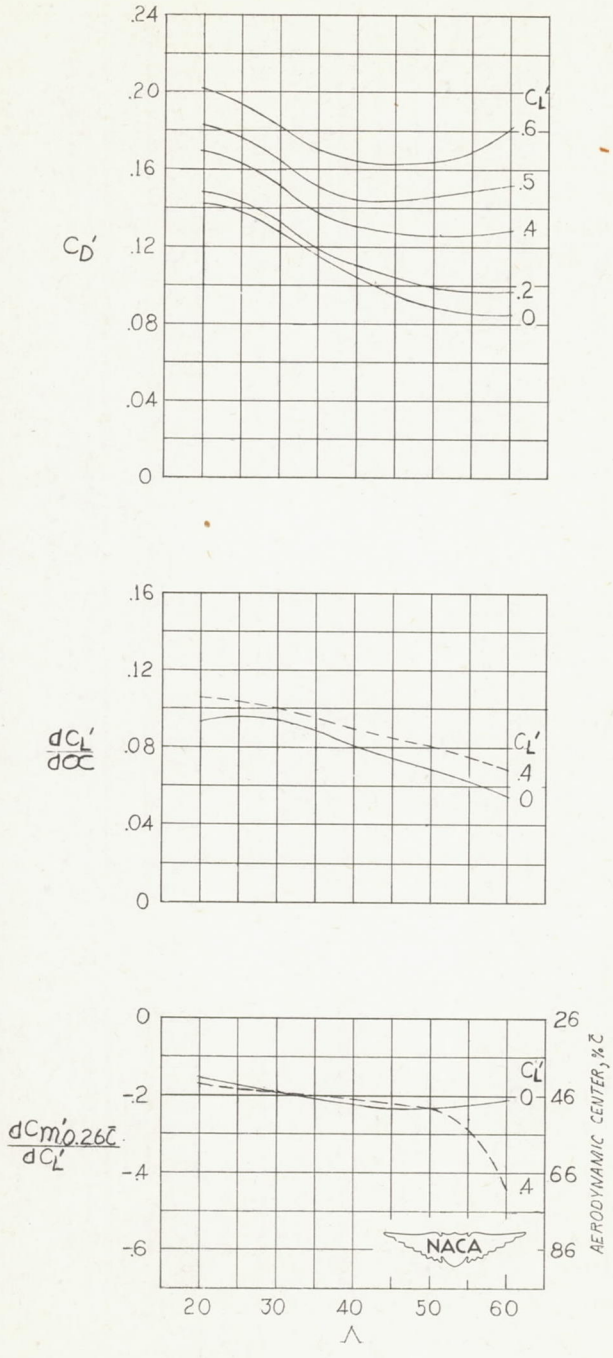
(d) M = 0.90.

Figure 13.- Continued.



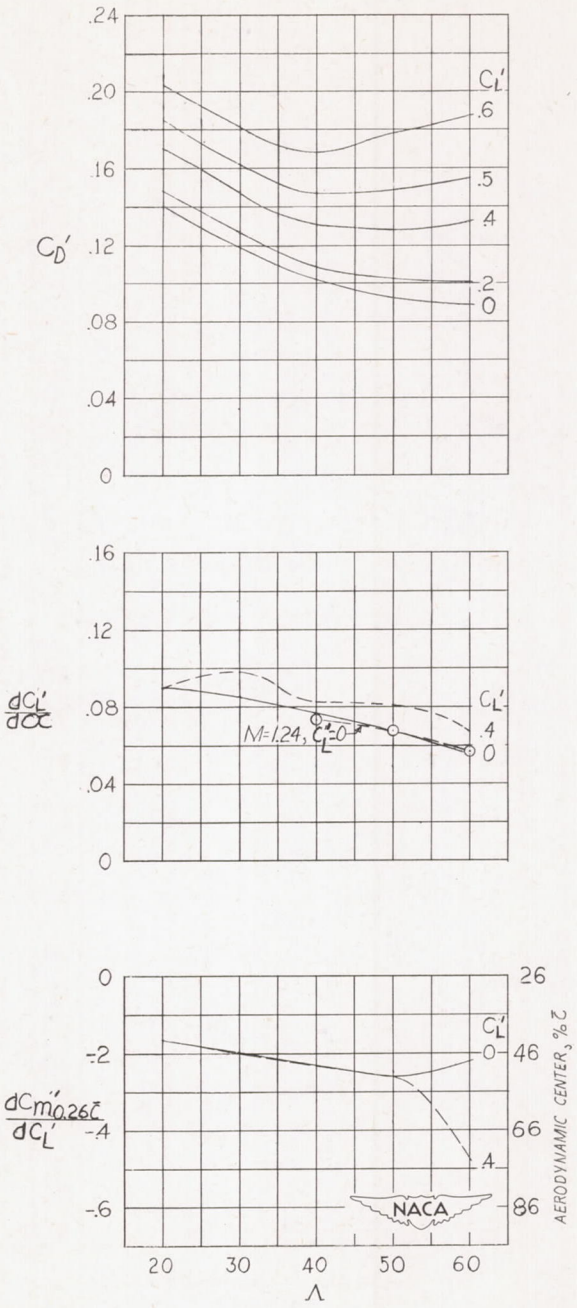
(e) M = 0.95.

Figure 13.- Continued.



(f) M = 1.00.

Figure 13.- Continued.



(g) M = 1.03.

Figure 13.- Concluded.

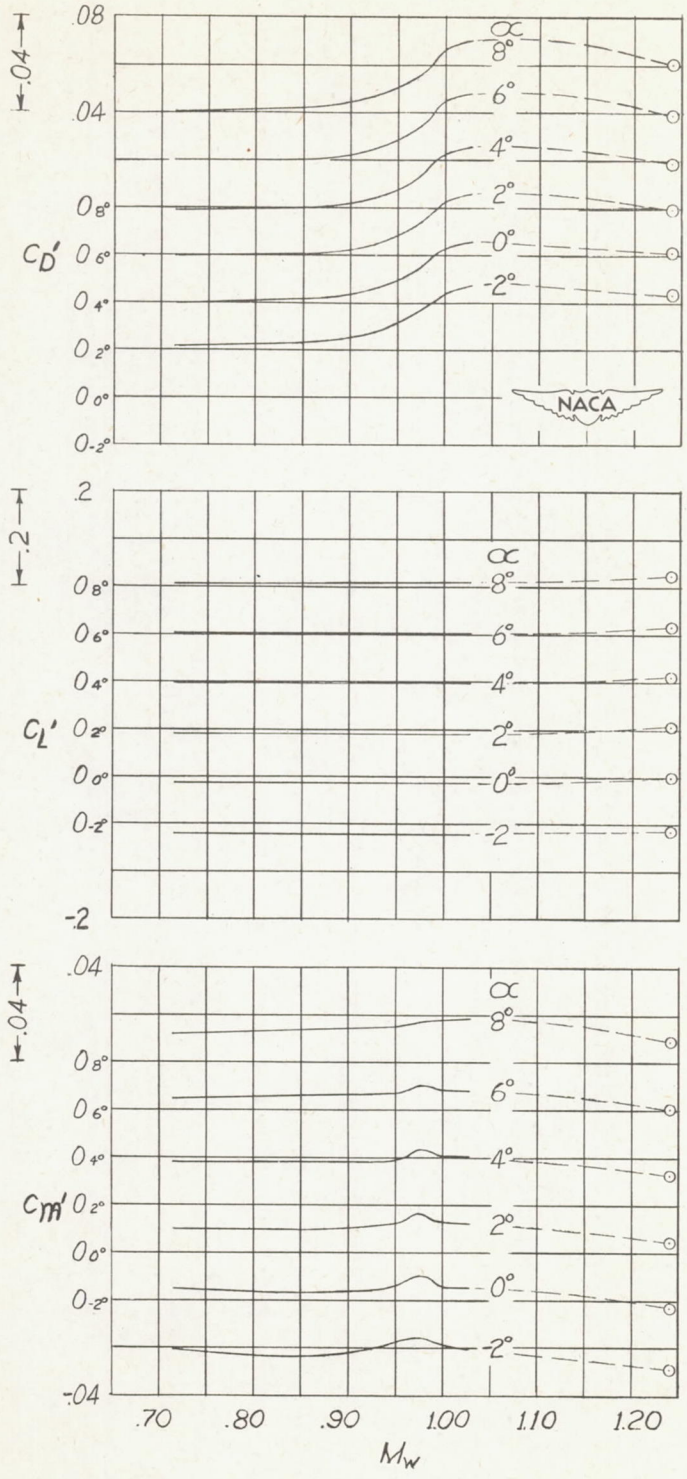


Figure 14.- Variation of lift, drag, and pitching-moment coefficients with Mach number at several values of angle of attack of a Bell X-5 semispan model of fuselage alone.

NACA-Langley - 11-14-52 - 350